INTERNATIONAL JOURNAL OF ENVIRONMENT, ENGINEERING & EDUCATION

ISSN 2656-8039 (ONLINE)
VOLUME 8 • ISSUE 3 • SEPTEMBER 2026

Received: 23 December 2025 | Accepted: 12 September 2026 | Published: 18 September 2026

Research Article

Reconstructing and Projecting Urban Expansion in Makassar Using Integrated ANN–CA and Bayesian Weights of Evidence, 2005–2035

Muh. Rais Abidin [a,b,*] • Andang Suryana Soma [c] • Arifuddin Akil [d] • Eymal Bashar Demmallino [a] • Muhammad Alimuddin Hamzah Assegaf [e] • M. Ramli AT [f]

[a] Department of Environmental Science, Hasanuddin University, Makassar, Indonesia | [b] Department of Geography, Universitas Negeri Makassar, Makassar, Indonesia | [c] Department of Forestry, Hasanuddin University, Makassar, Indonesia | [d] Department of Urban and Regional Planning, Hasanuddin University, Makassar, Indonesia | [e] Department of Geophysics, Hasanuddin University, Makassar, Indonesia | [f] Department of Sociology, Hasanuddin University, Makassar, Indonesia

ABSTRACT

Coastal urbanization requires spatial models that distinguish historical change from conditional projections. This study reconstructed land-use and land-cover dynamics in Makassar, Indonesia, from 2005 to 2025 and projected built-up expansion to 2035 using an integrated artificial neural network–cellular automata (ANN–CA) framework and Bayesian Weights of Evidence (WoE). Five Landsat-derived maps were classified into seven classes using Random Forest, with reported overall accuracy ranging from 62.83% to 87.61%. Ten demographic, accessibility, economic, topographic, and environmental variables were used to estimate transition potential and interpret factor-class associations. Model performance was evaluated using Kappa and the Figure of Merit. Built-up land increased from 8,199.20 ha in 2005 to 9,880.06 ha in 2025, a net gain of 1,680.86 ha (20.50%), while its share of the study area rose from 46.61% to 56.17%. Expansion decelerated sharply: 93.48% of the observed net increase occurred during 2005–2015. Cropland recorded the largest net decline (861.81 ha), whereas wetlands and water bodies jointly declined by 607.87 ha. Population growth and land value showed the strongest positive summarized contrasts, while the flood-exposure variable showed the strongest negative contrast. Kappa reached 0.768, but the Figure of Merit was 21.01%, indicating stronger whole-map agreement than locational accuracy for changed cells. Built-up land is projected to reach 10,394.23 ha (59.09% of the study area) by 2035, with 93.38% of projected growth occurring after 2030. The results provide a conditional basis for spatial screening of development pressure, but mapping uncertainty, uneven temporal allocation, and limited locational accuracy require cautious planning interpretation.

KEYWORDS coastal spatial planning • figure of merit (FoM) • land-use and land-cover change • landsat time series • random forest classification • transition-potential modeling

ARTICLE CITATION
M. R. Abidin, A. S. Soma, A. Akil, E. B. Demmallino, M. A. H. Assegaf, M. Ramli AT "Reconstructing and Projecting Urban Expansion in Makassar Using Integrated ANN–CA and Bayesian Weights of Evidence, 2005–2035," International Journal of Environment, Engineering and Education, Vol. 8, No. 3, pp. 447-473, 2026. https://doi.org/10.55151/ijeedu.v8i3.397

***CORRESPONDENCE**
Muh. Rais Abidin muhraisabidin@unm.ac.id Department of Environmental Science, Post-Graduate Program, Hasanuddin University, UNHAS Tamalanrea Campus, Perintis Kemerdekaan KM. 10 Road, Makassar, Sulawesi Selatan 90245, Indonesia https://orcid.org/0000-0002-6294-0685

1. INTRODUCTION

Urban expansion is defined here as the conversion of non-built-up land into built surfaces and constitutes the physical land-cover expression of urbanization. It must be distinguished from urban sprawl, which denotes a particular expansion morphology characterized by low density, discontinuity, fragmentation, functional separation, or excessive land consumption; expansion can also occur through contiguous edge growth or compact infill [1]–[3]. This distinction is analytically consequential because equal increments of built-up land may produce markedly different effects on infrastructure efficiency, accessibility, ecological continuity, and social exposure. Population and economic growth remain major aggregate drivers of urban land demand, but their relative influence differs across regions, development stages, and governance conditions [4], [5]. Uncoordinated expansion can irreversibly replace agricultural and natural land, fragment habitats, alter hydrological and biogeochemical processes, and displace environmental pressure beyond the urban boundary [6], [7].

Urban expansion is temporally uneven and spatially anisotropic, as cities may alternate among accelerated outward conversion, deceleration, consolidation, and renewed peripheral growth [3], [5]. Development may cluster along transport corridors and existing settlements or emerge as infill, edge expansion, and isolated leapfrog patches [8]. Aggregate area change therefore quantifies expansion magnitude but obscures its timing, direction, concentration, and morphology. The long, radiometrically calibrated Landsat archive enables consistent reconstruction of these dimensions across repeated observations [9], [10], while global mapping confirms substantial intra- and interurban variation in growth rates and configurations [3]. Historical change detection remains retrospective and cannot independently identify future conversion locations. Planning therefore requires a spatially explicit modeling framework that learns transition relationships from observed change and allocates subsequent urban growth according to local suitability, accessibility, and neighborhood effects [11].

Transition locations emerge from interacting demand, accessibility, physical suitability, market incentives, and regulatory constraints [12], [13]. Population growth raises land demand, whereas density may indicate agglomeration or scarce convertible land, producing spatially variable effects [13]. Land value combines accessibility, conversion costs, expected rents, and development expectations; high values may attract investment, while prohibitive acquisition costs delay conversion [14]. Proximity to roads, employment centers, and public services lowers access costs and channels peripheral development [15]. Elevation, slope, land cover, and river proximity condition feasibility and hazard exposure. In low-lying coastal cities, accessible sites may remain exposed to flooding and riverine processes [16]–[18]. Driver effects should therefore be estimated locally and interpreted as context-dependent spatial associations, not universal causal relationships [13].

Cellular Automata (CA) models are suitable for this task because they represent land conversion as iterative changes in cell state governed by transition potential, neighborhood effects, demand, and exclusion rules. Their credibility nevertheless depends on how transition rules are estimated. Fixed or linear rules can inadequately represent thresholds and interactions among demographic, economic, accessibility, and environmental variables. Artificial Neural Networks (ANNs) can learn nonlinear transition functions from observed changes, after which CA allocates projected demand while preserving local spatial dependence [11]. ANN–CA applications have produced spatially explicit LULC forecasts in Indonesia and other rapidly urbanizing settings [19], [20]. Predictive flexibility does not ensure explanatory clarity: ANN-derived probabilities may remain difficult to interpret and can be sensitive to class imbalance, calibration-period selection, underfitting, overfitting, and temporal non-stationarity.

Bayesian Weights of Evidence (WoE) provides a complementary diagnostic rather than a substitute predictive model. WoE compares the prior and conditional odds of observed transitions within each class of an evidential factor; positive contrast indicates association with conversion, negative contrast indicates inhibition, and values near zero indicate weak discrimination [21]. This class-specific representation makes nonlinear distance ranges and environmental thresholds more interpretable, although it does not establish causation and requires attention to dependence among explanatory layers. Used alongside ANN–CA, WoE separates two questions that are often conflated: how accurately future change can be allocated and which observed spatial conditions are associated with that change [22], [23]. Validation must make the same distinction. Kappa summarizes categorical agreement but may be dominated by persistent cells, whereas the Figure of Merit (FoM) evaluates overlap among observed and simulated change pixels [24], [25]. Reporting both metrics therefore provides broader evidence than either statistic alone.

Makassar provides a policy-relevant test of this framework. The city is the economic core of the MAMMINASATA metropolitan region, and its expansion redistributes settlement and commercial activity across a densely connected coastal–peri-urban system. Remote-sensing studies identified substantial built-up growth, particularly toward northern Makassar, while metropolitan analyses documented corridor-oriented and concentric expansion into surrounding areas [26], [27]. A CA–Markov study subsequently projected continued conversion in the Tamalanrea and Biringkanaya peri-urban districts, confirming that development pressure extends beyond the established core [28]. These changes have environmental implications. Surface-water monitoring detected losses and reconfiguration associated with reclamation and settlement development [27], and a 29-year Landsat analysis linked recent urbanization to increasing heat exposure while identifying protective effects of green and blue space [29]. Hydrologic–hydrodynamic modeling further shows that Makassar's low-lying coastal and riverine areas remain exposed to interacting flood contributions from the Jeneberang and Tallo systems [30].

Despite this evidence, the Makassar literature remains analytically fragmented. Previous studies have mapped built-up change, examined metropolitan sprawl, evaluated environmental consequences, or projected selected peri-urban districts. However, they have not jointly reconstructed city-wide change over five observation years, estimated nonlinear transition potential, interpreted factor-class associations, and evaluated simulated change using complementary agreement measures. Because an integrated ANN–CA–WoE design has recently been demonstrated elsewhere [31], the present study advances the approach through its context-specific application to Makassar, five-date temporal design, and evaluation of simulated transitions against an observed reference map. This extension is required because relationships among density, land value, accessibility, land availability, and hydrological constraint are conditioned by Makassar's particular metropolitan and coastal structure.

This study integrates Landsat-derived LULC maps for 2005, 2010, 2015, 2020, and 2025 with ANN–CA simulations for 2030 and 2035. Ten spatial drivers are evaluated across four domains: environmental and topographic conditions, demographic pressure, accessibility, and economic attractiveness. The analysis addresses four questions: (1) how did the magnitude, rate, and spatial form of LULC change vary between 2005 and 2025; (2) where is built-up expansion most likely to occur by 2030 and 2035; (3) which factor classes favor or inhibit transition to built-up land; and (4) how reliably does the model reproduce the observed quantity and location of change? By linking multi-period observation, nonlinear transition estimation, interpretable Bayesian evidence, and change-specific validation, the study provides a reproducible basis for identifying development pressure, prioritizing growth-management zones, and directing future conversion away from environmentally constrained locations.

2. LITERATURE REVIEW

2.1. Spatiotemporal Dynamics of Urban Expansion

Urban expansion denotes conversion of non-built land into built surfaces, whereas urban sprawl is a spatial form marked by low density, discontinuity, fragmentation, and peripheral extension. Compact infill can increase built-up area without intensifying sprawl; the same increment dispersed among isolated patches can do so [32], [33]. Analysis must therefore separate the amount, timing, and location of conversion from the configuration and land-use efficiency of the resulting urban form.

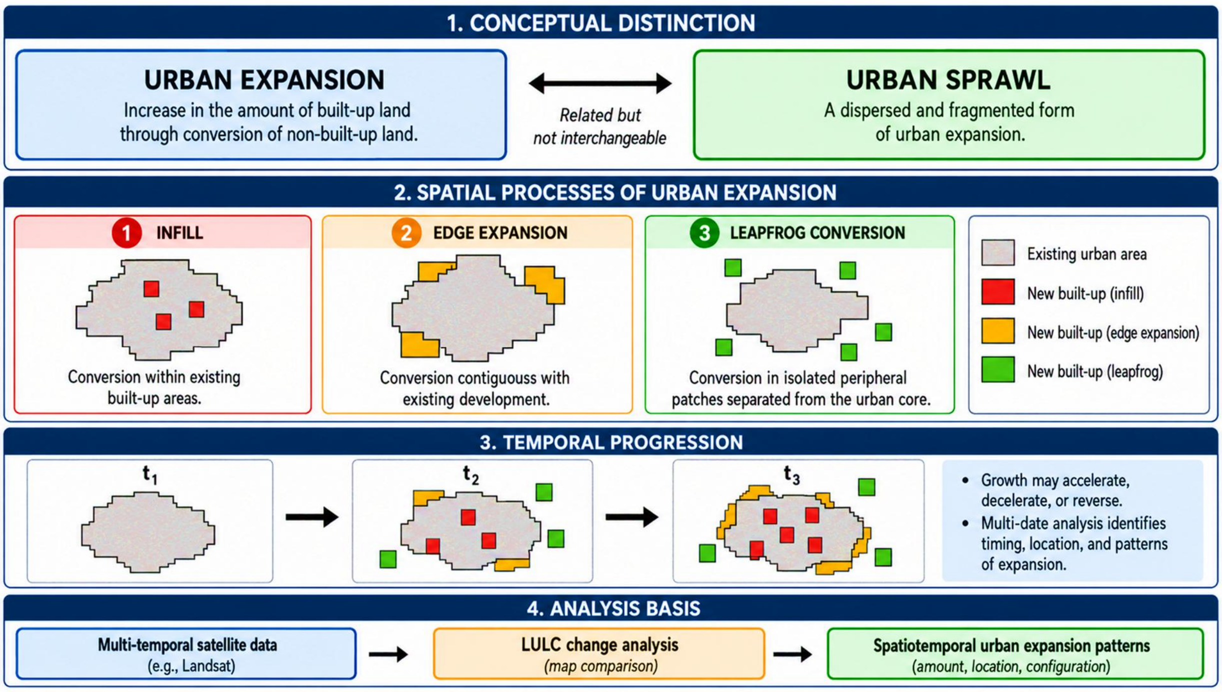

Figure 1. Conceptual framework of urban expansion as a spatiotemporal land-change process. Adapted from Martinuzzi et al. [34]; El Garouani et al. [35]; Gaur et al. [36]; Wang et al. [37]; and de Abreu e Silva and Correia [2].

Infill, edge expansion, and leapfrog development describe conversion within, contiguous to, and separate from existing built-up areas. Their relative dominance changes across phases of outward growth, consolidation, and renewed peripheral development [34], [35], [37]. Net change alone cannot distinguish compact from fragmented trajectories, while long intervals can mask acceleration, deceleration, or directional reversal [36], [38]. Multi-date analysis is required to identify when and where growth occurs and whether new development remains connected to the urban fabric.

Long-term Landsat series provide consistent medium-resolution coverage, while GIS supports map comparison, transition measurement, and integration of explanatory variables [35], [36], [39]. Spatiotemporal inference nonetheless depends on comparable class definitions, seasonal consistency, geometric alignment, and explicit accuracy assessment; otherwise, classification errors propagated across dates may be mistaken for real conversion [36], [40].

Expansion effects depend on scale and configuration. Fringe conversion can reduce cropland, fragment open areas, alter runoff, raise surface temperature, and weaken ecosystem services [41]–[44]; dispersed development can increase infrastructure and travel demands while producing unequal access and environmental exposure [32], [45], [46]. These risks are acute in coastal cities where urban demand intersects with low elevation, flooding, river systems, and scarce suitable land [47], [48]. Assessment must connect observed conversion to locational attraction, availability, and constraint.

2.2. Multidimensional Drivers of Urban Expansion

Urban expansion reflects interacting demand, accessibility, physical suitability, and regulatory or environmental constraints. No universal driver hierarchy applies: associations vary by scale, development stage, institutions, and period [49], [50]. Cell-level models approximate these mechanisms through spatial proxies: demographic and economic variables indicate demand, accessibility structures locational advantage, and biophysical conditions delimit feasible conversion.

2.2.1. Demographic Pressure and Spatial Saturation

Population growth is a flow variable indicating additional demand for housing, services, employment, and infrastructure, and is commonly associated with conversion near established areas and accessible corridors [50]–[53]. Density is a stock variable. It may support agglomeration and redevelopment, or signal land scarcity, high acquisition costs, and saturation that displace development toward the periphery [2], [49]. The variables represent related but distinct processes.

Jointly modeling growth and density distinguishes rapidly expanding peripheral zones from mature, densely occupied neighborhoods. Growth should generally correspond to incremental demand, whereas density may attract development or redirect it outward when saturation dominates. This separation limits erroneous attribution of peripheral conversion to population level when redistribution of new growth is the operative process [37], [52].

2.2.2. Accessibility, Economic Centers, and Land Markets

Accessibility lowers the temporal and monetary costs of reaching employment, markets, services, and existing urban areas [54], [55]. Road proximity can increase locational advantage and development potential [50], [56], [57], redirect growth to the periphery, and generate corridor expansion [58], [59]. Causality remains reciprocal: roads may stimulate conversion, while urban expansion induces infrastructure provision [60], [61]. Distance to roads is thus an accessibility proxy, not direct causal evidence.

Economic centers concentrate employment, trade, and investment; service centers concentrate education, health care, administration, and other urban functions. Although proximity to both may increase transition potential, their spatial reach can differ [2], [57]. Polycentric development may redirect conversion toward secondary centers, while improved transport extends their influence [62], [63]; separate distance measures are preferable to a generic centrality variable.

Land value integrates accessibility, expected returns, infrastructure, development rights, and scarcity. High values may indicate profitable conversion at the urban edge, yet acquisition costs can redirect land-intensive development to cheaper peripheral parcels [49], [64]. Effects also depend on whether values represent pre-conversion markets, assessments, or interpolated transactions. Land value should be treated as an empirically estimated indicator of economic attractiveness rather than an invariably positive driver.

2.2.3. Physical Suitability, Hydrological Constraints, and Open-Space Availability

Elevation and terrain affect drainage, foundations, infrastructure design, and access. Their discriminatory power is usually greater in complex terrain, but small elevation differences can remain important in flat cities through flood susceptibility [48], [65]. Elevation is a locally conditioned suitability variable whose meaning depends on relief and hydrological interaction.

Hydrological variables require separation. River proximity can confer amenity or economic access, yet may indicate inundation, erosion, riparian restrictions, or poor drainage. Flood exposure generally raises construction and damage costs [16], [17], [48], although scarcity, weak enforcement, informal settlement, or protective infrastructure may sustain conversion. River location represents network context; flood exposure represents hazard intensity.

Protected green space constrains conversion, whereas unprotected vegetation or vacant land can represent remaining developable supply. A positive association between open land and conversion therefore indicates opportunity or development pressure, not ecological causation [41], [66]. This distinction matters where green-space loss coincides with higher surface temperatures and declining environmental quality [40]. Protection status and classification metadata must prevent land availability from being equated with planning permission.

2.2.4. Interaction and Spatiotemporal Heterogeneity

Parcel selection is conditional: low cost cannot offset severe inaccessibility, and high accessibility may not compensate for flood risk. Conversion can accelerate when population growth, roads, services, and land values align, producing thresholds and nonlinearities poorly captured by additive linear specifications [49], [50]. Built-up neighbors add feedback by facilitating infrastructure extension and strengthening expectations of adjacent development.

Driver effects can change over time. Expansion may initially follow roads, later fill intervening land, and eventually shift to constrained sites after suitable parcels are exhausted [37], [38]. Historical calibration assumes partial persistence of these relationships. Multiple observation dates reveal, but cannot eliminate, temporal instability; interpretation must remain bounded by the input period and resolution, even when the model captures interactions.

2.3. ANN–CA Modeling of Urban Expansion

Cellular Automata (CA) simulate iterative state changes governed by current land use, neighborhood composition, suitability, and conversion rules, translating local interactions into diffusion, infill, edge expansion, and leapfrog patterns [19]. Markov chains are often used to estimate transition quantities and suitability procedures to allocate them spatially [67]–[69]. Fixed rules, however, may represent correlated demographic, economic, accessibility, and environmental responses inadequately.

Artificial Neural Networks (ANNs) estimate nonlinear relations between historical transitions and spatial predictors. In ANN–CA, the ANN produces transition potential, while CA allocates the required change using neighborhood influence and land-state constraints. Thus, ANN estimates where conversion is comparatively likely and CA represents its spatial propagation. Applications across Indonesia, China, Kuwait, and coastal metropolitan regions demonstrate the flexibility of this hybrid structure [19], [47], [70], [71].

Predictive flexibility requires control. ANN outputs depend on data quality, temporal alignment, predictor specification, network architecture, and separation of calibration from validation [20], [71]. Excess capacity may learn noise or redundant information, and class imbalance may favor persistence when unchanged cells dominate [72]. More complex neural CA models can capture heterogeneity and temporal dependence, but complexity does not ensure interpretability or transferability [73]. Driver selection must remain theoretically grounded because predictive association is not causal explanation [74].

Forecast relationships may weaken when demographics, infrastructure, regulation, hazards, or economic conditions change. ANN–CA outputs are conditional scenarios, not deterministic futures; credibility depends on temporal validation, explicit constraints, and disclosure of represented and omitted processes [47], [57]. Their defensible planning use is to locate comparatively high conversion pressure and test its conflict with environmental or service-capacity constraints.

2.4. Bayesian Weights of Evidence (WoE)

Because ANN–CA prioritizes prediction and allocation, its learned weights do not directly explain individual drivers. Bayesian Weights of Evidence (WoE) provides class-specific, frequency-based interpretation: positive and negative weights compare transition with non-transition, and their contrast indicates association direction and strength [21], [75]. Positive contrast denotes overrepresentation among converted cells; negative contrast denotes relative avoidance. Magnitudes remain conditional on the classification, spatial unit, and estimation period.

WoE can reveal non-monotonic responses across road-distance bands, land-value ranges, or flood-exposure levels that a single coefficient conceals. Studentized contrast distinguishes stronger evidence from sparse patterns, while a continuity correction stabilizes zero cells [76]. These procedures strengthen interpretation without converting association into causation.

WoE assumes sufficient conditional independence among evidence layers; dependence among accessibility, land value, and economic-center proximity can duplicate information. Results also depend on discretization: broad classes conceal thresholds, whereas narrow classes yield unstable counts. Correlation screening, defensible boundaries, and local knowledge are therefore required [31]. ANN estimates joint nonlinear transition potential; WoE interprets bivariate factor-class support or inhibition.

2.5. Validation of Spatial Change Simulation

Validation must separate whole-map agreement from agreement on changed locations. Kappa adjusts observed agreement for chance but can be inflated when correctly simulated persistence dominates [77], [78]; high values may therefore coexist with poor identification of new built-up land. Kappa remains useful as a global diagnostic when complemented by Figure of Merit (FoM) and explicit allocation-error analysis [79].

FoM evaluates changed cells through hits, misses, false alarms, and wrong hits, excluding correctly predicted persistence. It therefore tests land-change performance more stringently than measures dominated by stable cells [25], [79], [80]. Error decomposition indicates whether deficiencies concern change quantity or location. Joint reporting is complementary: Kappa assesses overall map correspondence, whereas FoM evaluates the smaller, policy-relevant transition domain.

Credible forecasting calibrates an earlier transition, reproduces a later observed map, evaluates overall and change-specific agreement, and only then projects beyond observation. Temporal separation reduces circular validation but cannot test future structural breaks. Spatial error should also be examined around fringes, rivers, and flood-prone zones, since acceptable aggregate scores can conceal systematic planning-relevant failure [48], [80].

2.6. Research Synthesis and Analytical Framework

Makassar studies document built-up expansion and densification alongside green-space pressure, surface-temperature change, and altered inland-water conditions [27], [40], [81]. Nevertheless, descriptive maps do not locate future expansion, predictive models do not inherently interpret drivers, and whole-map validation may exaggerate performance when persistence dominates. A unified framework is required to connect historical change, projected exposure, driver interpretation, and model reliability.

Built-up conversion is represented through four interacting domains: demographic pressure, accessibility, economic attractiveness, and physical-environmental conditions. Growth and proximity to roads, services, and economic centers should raise transition potential; flooding and adverse hydrology may inhibit it. Density, elevation, land value, and green/open space remain conditional indicators of attraction, supply, saturation, cost, protection, or constraint [49], [64], [66].

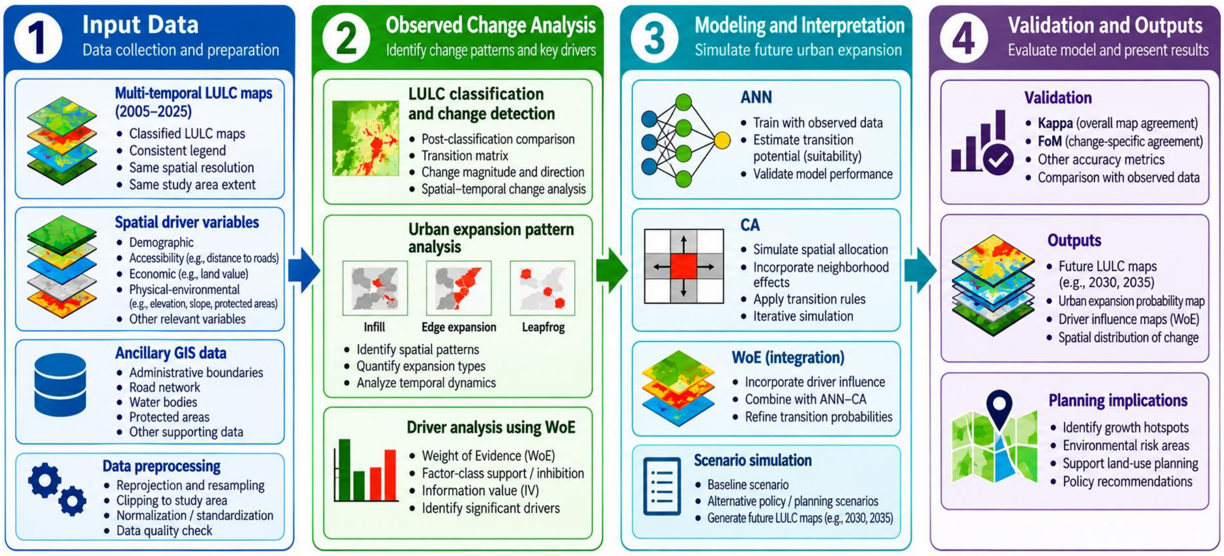

Figure 2. Analytical framework for urban expansion analysis and simulation.

Each component has a distinct role. Multi-temporal LULC analysis measures observed change; ANN estimates nonlinear transition potential; and CA allocates change under neighborhood and land-state constraints. WoE identifies supportive or inhibitory factor classes, while Kappa and FoM assess overall and change-specific agreement. The framework separates description, prediction, interpretation, and validation, treating projections as conditional pressure rather than inevitable outcomes.

Five-year observations from 2005–2025 and projections for 2030 and 2035 are used to evaluate Makassar's built-up expansion, future allocation, associated drivers, and reliability against observed change, extending retrospective mapping into an interpretable, explicitly validated model.

3. MATERIALS AND METHODS

3.1. Study Area

The modeling extent followed the administrative boundary of Makassar City, South Sulawesi Province, Indonesia. Makassar is the principal urban and economic center of eastern Indonesia and the core city of the MAMMINASATA metropolitan region. Maros Regency borders the municipality to the north, Gowa Regency to the east and south, Takalar Regency to the southwest, and the Makassar Strait to the west. The study boundary therefore represents the metropolitan core rather than the entire MAMMINASATA conurbation. This distinction is retained throughout the analysis to avoid attributing municipal-scale results to the full metropolitan territory.

Makassar is predominantly low-lying and has a relatively gentle topographic gradient. Its coastal position, river network, flood exposure, rapid demographic change, and concentration of transport and economic functions create spatially competing development incentives and constraints. Previous studies document sustained built-up expansion and peri-urban conversion in Makassar, supporting its suitability for spatiotemporal urban-expansion modeling [28], [40], [82].

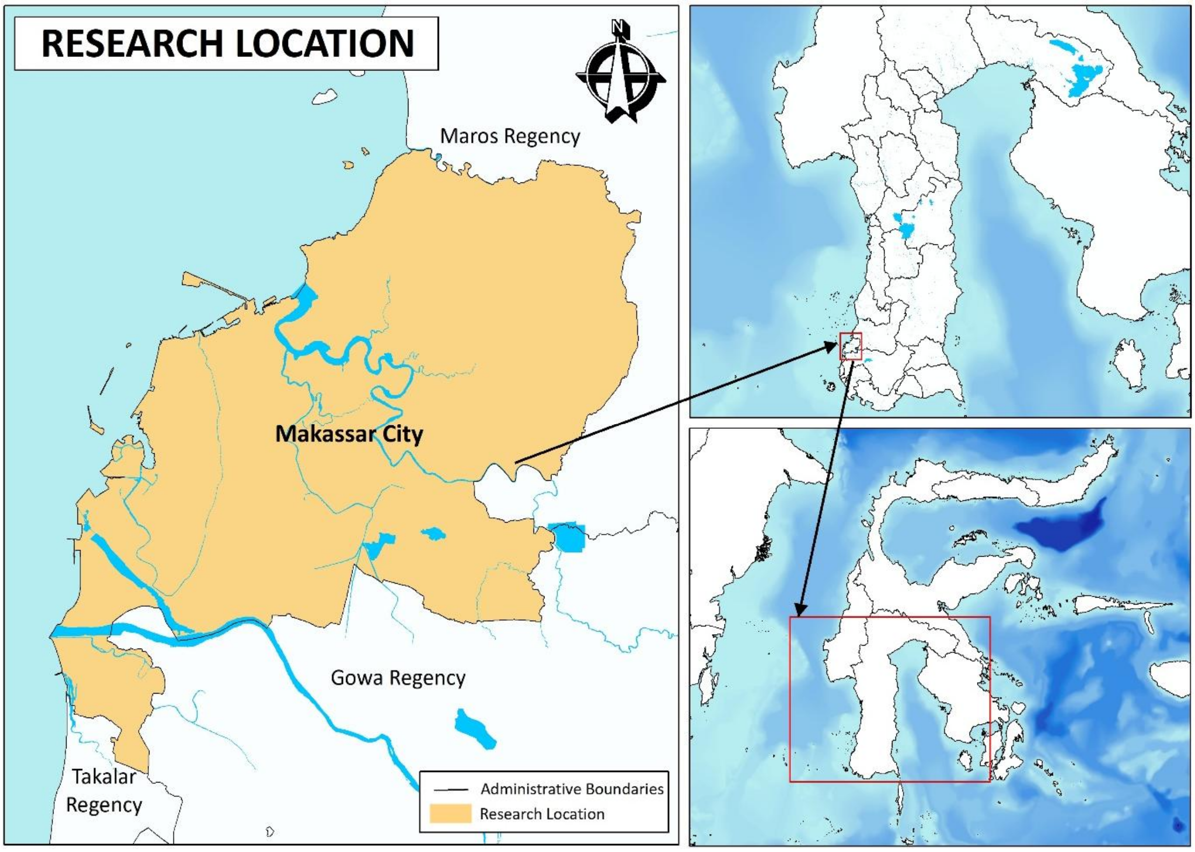

Figure 3. Location of the study area in Makassar City, South Sulawesi, Indonesia.

3.2. Research Design and Analytical Workflow

The study employed a retrospective and predictive spatial design to reconstruct urban land transformation, estimate the probability of conversion to built-up land, and allocate future change. Five land-use/land-cover (LULC) observations representing 2005, 2010, 2015, 2020, and 2025 formed the temporal basis of the analysis. The observed series was used for post-classification change detection and for constructing transition samples. Projections were subsequently produced for 2030 and 2035. This design separates four analytical functions: description of historical change, estimation of nonlinear transition potential, spatial allocation of projected conversion, and interpretation of driver associations (Figure 4).

The raster cell constituted the unit of analysis. Each cell contained its LULC state at time t, its neighborhood condition, and values for ten demographic, accessibility, economic, and physical-environmental variables. The Artificial Neural Network (ANN) estimated cell-level transition potential, and the Cellular Automata (CA) component allocated change according to that potential, local neighborhood effects, conversion constraints, and the quantity of change specified by the model. Bayesian Weights of Evidence (WoE) was applied independently to characterize the direction and strength of spatial associations between factor classes and observed built-up transitions. Model evaluation used Kappa and Figure of Merit (FoM), which assess whole-map agreement and change-specific agreement, respectively [80].

3.3. Data Sources and Spatial Preprocessing

3.3.1. Multi-temporal satellite observations

Multi-temporal Landsat imagery was used to derive comparable LULC maps across the twenty-year observation period. One scene represented each target year, with a nominal multispectral resolution of 30 m (Table 1). Where a native panchromatic band was available, pan-sharpening was used to generate a 15 m spatial product for visual and classification support. Pan-sharpening combines multispectral information with the finer spatial detail of a panchromatic band; its effect depends on sensor characteristics, fusion method, and classifier, and it does not create additional spectral information [83]. The scenes were clipped to the study area.

Temporal comparability requires consistent spectral preparation and geometric registration. The archived processing documentation did not specify the reflectance product level, atmospheric-correction procedure, cloud and shadow masking, Landsat 7 ETM+ gap-filling procedure, pan-sharpening algorithm, or residual co-registration error. These omissions limit exact replication of the LULC workflow [36].

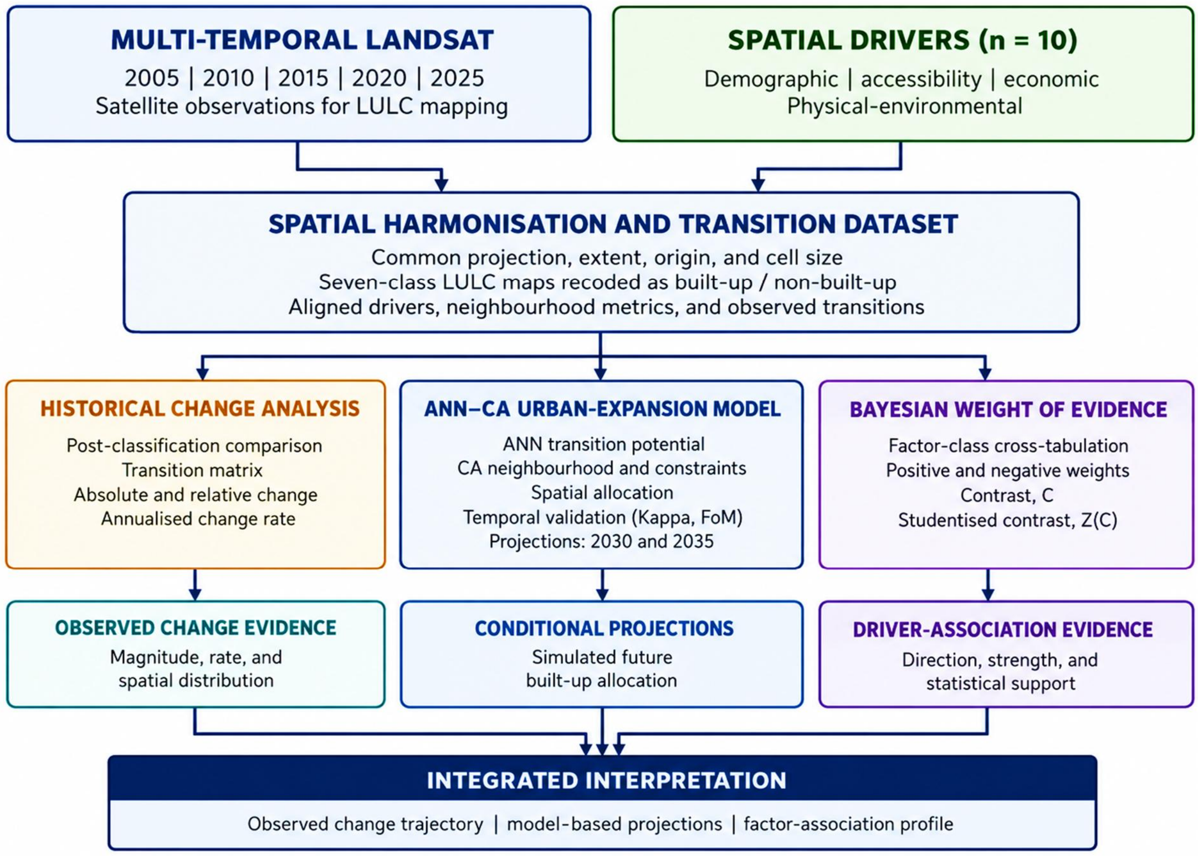

Figure 4. Analytical workflow integrating LULC change analysis, ANN–CA urban-expansion modeling, Bayesian Weights of Evidence, model validation, and conditional projection.

3.3.2. Spatial driving factors

Ten explanatory layers were selected across four domains. Population density and population growth represented demographic conditions. Distance to major roads and service centers represented accessibility. Distance to economic centers and land value represented economic attractiveness. Elevation, distance to rivers, flood exposure, and distance to protected or green open space represented physical and environmental conditions. The selection reflects evidence that urban conversion is jointly conditioned by demographic demand, transport access, economic centrality, land-market conditions, terrain, and environmental constraints [65].

Each source layer was transformed into a raster compatible with the LULC grid. Distance-based variables were represented by the analytical classes listed in Table 2, while elevation, flood exposure, population attributes, and land value retained their specified intervals. Raster origin, cell size, extent, projection, and no-data mask were held constant across model inputs. However, the archived processing documentation did not specify the ArcGIS version, distance algorithm, resampling rule, or reference year for each time-varying driver. These omissions limit exact replication of the spatial preprocessing.

Table 1. Multi-temporal Landsat observations used in the temporal analysis.

Year	Satellite and sensor	Native spatial resolution	WRS path/row	Analytical role
2005	Landsat 5 TM	30 m multispectral	114/64	Baseline LULC map
2010	Landsat 7 ETM+	30 m multispectral; 15 m panchromatic	114/63	Intermediate LULC map
2015	Landsat 8 OLI/TIRS	30 m multispectral; 15 m panchromatic	114/64	Intermediate LULC map
2020	Landsat 8 OLI/TIRS	30 m multispectral; 15 m panchromatic	114/64	Intermediate LULC map
2025	Landsat 9 OLI-2/TIRS-2	30 m multispectral; 15 m panchromatic	114/64	Most recent observed LULC map

Table 2. Spatial driving factors, operational classes and data sources.

Domain	Variable	Operational classes	Data source
Physical-environmental	Elevation	1–10 m; 11–40 m; 41–90 m	Geospatial Information Agency of Indonesia [84]
	Distance to river network	<1 km; 1–3 km; >3 km	Geospatial Information Agency of Indonesia [84]
	Flood exposure	Flood-prone (Unsuitable/Moderately suitable); Flood-prone (Moderately suitable); Not flood-prone (Highly suitable)	BNPB InaRISK [84]
	Distance to protected/green open space	<500 m; 500–1,000 m; >1,000 m	Ministry of Forestry [86]
Demographic	Population density	≤50 inhabitants/km² (Very low density); 51–250 inhabitants/km² (Low density); 251–400 inhabitants/km² (Moderate density); ≥401 inhabitants/km² (Very high density)	BPS Statistics of Makassar Municipality [87]
	Population growth	0.0% to <0.5% (Very low); 0.5% to <1.0% (Low); 1.0% to <2.0% (Moderate); 2.0%–3.0% (High); >3.0% (Very high)	BPS Statistics of Makassar Municipality [87]
Accessibility	Distance to major roads	<1 km; 1–6 km; >6 km	OpenStreetMap [88]
	Distance to service centers	<1 km; 1–6 km; >6 km	OpenStreetMap [88]
Economic	Distance to economic centers	<1 km; 1–6 km; >6 km	OpenStreetMap [88]
	Land value	< IDR 500,000/m² (Very low); IDR 500,000 to < IDR 1,000,000/m² (Low); IDR 1,000,000 to < IDR 2,000,000/m² (Moderate); IDR 2,000,000 to < IDR 5,000,000/m² (High); ≥ IDR 5,000,000/m² (Very high)	ATR/BPN land-value-zone data [89]

The class intervals were treated as analytical bins rather than predetermined causal effects. Proximity to roads, services, and economic centers can indicate lower access costs, while population growth can represent incremental land demand [90]. Flood exposure may constrain formal development, and green/open-space proximity may represent either environmental protection or available land subject to conversion pressure [91]. The empirical sign of each class was therefore estimated through WoE rather than inferred from the ordering of the analytical classes.

3.4. LULC Mapping and Change Detection

3.4.1. LULC Classification and Accuracy Assessment

A supervised classification was used to generate LULC maps for 2005, 2010, 2015, 2020, and 2025. Seven classes were mapped: cropland, forest, shrubland, grassland, wetland, water bodies, and urban/built-up land. Class definitions followed the FAO Land Cover Classification System principles of Di Gregorio and Jansen [92]. They were limited to categories that could be consistently distinguished from Landsat imagery across all observation years.

Classification was implemented in Google Earth Engine using a Random Forest classifier. Random Forest aggregates decorrelated decision trees and can represent nonlinear class boundaries without imposing a parametric response form, while Google Earth Engine provides the cloud-computing environment used for large-scale geospatial processing [93], [94]. Training labels were assembled from TimeMark-geotagged field observations and medium-resolution reference maps and were distributed across the study area to represent the spectral and spatial variability of each LULC class.

Table 3. Thematic LULC classes and binary recoding used for urban-transition modeling.

Thematic class	Operational description	Binary model class
Cropland	Cultivated agricultural fields and managed crop areas	Non-built-up
Forest	Areas dominated by tree cover	Non-built-up
Shrubland	Areas dominated by shrubs or low woody vegetation	Non-built-up
Grassland	Areas dominated by herbaceous vegetation	Non-built-up

Thematic class	Operational description	Binary model class
Wetland	Water-saturated or periodically inundated vegetated areas	Non-built-up
Water bodies	Rivers, reservoirs, and other open-water surfaces	Non-built-up
Urban/built-up	Residential, commercial, industrial, transport, and other impervious or constructed surfaces	Built-up

For the 2025 map, field-reference data were collected from 3 to 5 December 2025 at 379 locations; 268 locations were assigned to classifier training and 111 to independent validation. For the historical maps, for which temporally contemporaneous field observations were unavailable, reference labels were obtained from the Global Land Cover Change dataset using observations as close as possible to the corresponding Landsat acquisition date. Training and validation samples varied by year because reference availability and class representation differed among dates (Table 4).

After thematic classification, the seven LULC classes were recoded into a binary response for urban-transition modeling. Urban/built-up land formed the built-up class, whereas the remaining six classes formed the non-built-up class. This two-stage structure retained thematic information for historical change analysis while providing a consistent target for modeling non-built-up-to-built-up conversion.

Accuracy assessment used validation samples that were excluded from classifier training. The validation sample was selected using stratified sampling, and mapped and reference labels were cross-tabulated in an error matrix. Independent reference data, explicit sampling and response designs, and estimators consistent with the sampling design are required for rigorous thematic-map accuracy assessment [83], [95]. Overall Accuracy (OA), Producer's Accuracy (PA), and User's Accuracy (UA) are conventionally derived from the error matrix. The archived classification records do not include the underlying confusion matrices or documentation of any weighting scheme; consequently, the OA, PA, and UA values reported in Table 4 and Supplementary Table S1 are retained as source-record diagnostics and cannot be independently recalculated from the displayed sample counts.

$$OA = \frac{\sum_{i=1}^{k} n_{ii}}{N} \times 100 \quad (1)$$

$$PA_i = \frac{n_{ii}}{n_{i+}} \times 100 \quad (2)$$

$$UA_i = \frac{n_{ii}}{n_{+i}} \times 100 \quad (3)$$

For an unweighted error matrix, OA summarizes total agreement, PA is the complement of omission error, and UA is the complement of commission error. If sampling or area weights were applied in the archived classification records, the corresponding weighted estimators and denominators would be required to reproduce the reported percentages exactly.

Table 4. Training design and reported map-level classification accuracy by observation year.

Year	Platform and classifier	Training (n)	Validation (n)	OA (%)	Kappa
2005	GEE / Random Forest	278	117	62.83	0.50
2010	GEE / Random Forest	273	114	68.14	0.52
2015	GEE / Random Forest	283	124	68.14	0.50
2020	GEE / Random Forest	268	109	75.22	0.62
2025	GEE / Random Forest	268	111	87.61	0.81

Note: GEE = Google Earth Engine; OA = Overall Accuracy.

The class-level sample distribution and corresponding reported PA and UA values are provided in Supplementary Table S1. Classification accuracy was evaluated separately from ANN–CA validation. Table 4 and Supplementary Table S1 describe agreement between classified Landsat maps and reference labels, whereas the Kappa and Figure of Merit (FoM) reported for the ANN–CA simulation assess agreement between a simulated map and an observed LULC map. The two sets of Kappa statistics therefore represent different validation tasks and should not be interpreted interchangeably.

3.4.2. Post-classification Change Analysis

Post-classification comparison was used to identify cell-level transitions between successive observations and across the complete 2005–2025 interval. Cross-tabulation produced a transition matrix in which each entry records the area changing from class (j) at time (t_1) to class (k) at time (t_2). This approach permits direct identification of conversion to built-up land and avoids inferring a transition solely from independent changes in aggregate class area [35], [37]. For each class, absolute change was calculated as:

$$\Delta A = A(t_2) - A(t_1) \quad (4)$$

where $A(t_1)$ and $A(t_2)$ denote the class area at the beginning and end of the interval. Relative change was calculated as $100 \times \Delta A/A(t_1)$. Change detection quantified LULC transitions associated with urban expansion, including their magnitude, direction, and annualized rate between observation periods [96]. The annualized linear rate of change was estimated as:

$$r = \left[\frac{A(t_2) - A(t_1)}{A(t_1)}\right] \times \left[\frac{1}{t_2 - t_1}\right] \times 100 \quad (5)$$

where r is expressed as a percentage per year and $(t_2 - t_1)$ is the interval length in years. This measure is an annualized arithmetic rate, not a compound annual growth rate. The same definition was applied across intervals to preserve comparability.

3.5. ANN–CA Urban Expansion Model

3.5.1. Cellular State-Transition Structure

CA represents land change as an iterative update of discrete cell states. The state of cell (i) at time $(t + 1)$ is determined by its current state, the configuration of neighboring cells, and external spatial variables. The general transition rule is expressed as:

$$S_{i(t+1)} = f[S_{i(t)}, N_{i(t)}, X_i] \quad (6)$$

where $S_{i(t)}$ is the LULC state of cell (i) at time (t), $N_{i(t)}$ represents the selected neighborhood around that cell, (X_i) is the vector of ten spatial drivers, and (f) is the transition function. Neighborhood dependence permits local growth processes, including contiguous edge expansion and infill, to influence the allocation of new built-up cells [19], [97].

3.5.2. ANN Estimation of Transition Potential

The ANN replaced a fixed transition function with a data-driven estimator of nonlinear relationships. Training cases were derived from cells observed as non-built-up at the start of the calibration interval. The binary target distinguished cells that remained non-built-up from cells that converted to built-up land by the end of the interval. Predictor values comprised the ten driver layers together with the cell state and neighborhood information used by the implementation. The resulting transition potential was expressed as:

$$P_i(t \to t+1) = \text{ANN } [s_i(t), N_i(t), X_i] \quad (7)$$

where (P_i) is the estimated probability or relative potential of cell (i) converting to built-up land. ANN-based transition functions are suitable for interacting and non-monotonic predictors, but their estimates remain conditional on the sampling design, network configuration, and calibration period [20], [70].

3.5.3. CA Allocation, Temporal Validation, and Projection

The transition-potential surface generated by the ANN was supplied to the CA allocation stage. Candidate non-built-up cells were evaluated in relation to their transition potential, neighboring built-up configuration, and model constraints, and conversion was allocated iteratively until the required quantity of built-up change was reached. The retained implementation documentation did not specify the allocation rule, neighborhood definition, demand-estimation procedure, or iteration settings. These omissions limit exact replication of the allocation procedure.

Temporal validation preceded future projection. A model calibrated on an earlier transition interval was used to simulate an observed later year, and the simulated map was compared with its independent reference map. After the retained configuration had been evaluated, the 2025 LULC map served as the base state for projections to 2030 and 2035. These outputs represent conditional scenarios generated from historical relationships; they do not establish that the simulated conversions will occur [47], [71].

3.6. Bayesian Weights of Evidence Analysis

Bayesian WoE was used to quantify how strongly each class of a spatial factor was associated with observed conversion to built-up land. Let F denote membership in a specified factor class, T denote an observed non-built-up-to-built-up transition, and N denote the number of cells satisfying the stated condition. Positive and negative weights were calculated as [21]:

$$W^+ = ln\left(\frac{P(F \mid T)}{P(F \mid \bar{T})}\right) \quad (8)$$

$$W^- = ln\left(\frac{P(\bar{F} \mid T)}{P(\bar{F} \mid \bar{T})}\right) \quad (9)$$

where $(\bar{F})$ denotes cells outside the specified factor class and $(\bar{T})$ denotes cells that did not undergo the observed transition. The contrast for each factor class was calculated as:

$$C = W^+ - W^- \quad (10)$$

A positive contrast indicates that the class occurred proportionally more often among transition cells than among non-transition cells; a negative contrast indicates relative avoidance. These quantities express spatial association within the observed period and should not be interpreted as causal effects or as ANN connection weights [21], [31].

The conditional probabilities were estimated from the corresponding factor-class-by-transition cross-tabulation. A continuity correction of 0.5 was added to each cell of the 2 × 2 table when a sparse factor class produced a zero count. Sampling variances and the standard error of the contrast were calculated from the adjusted counts:

$$S^2(W^+) = \frac{1}{N(F \cap T)} + \frac{1}{N(F \cap \bar{T})} \tag{11a}$$

$$S^2(W^-) = \frac{1}{N(\bar{F} \cap T)} + \frac{1}{N(\bar{F} \cap \bar{T})} \tag{11b}$$

$$S(C) = \sqrt{S^2(W^+) + S^2(W^-)} \tag{11c}$$

Statistical support was assessed using the studentized contrast:

$$Z\,(C) = \frac{C}{S(C)} \tag{12}$$

Values satisfying $|Z(C)| > 1.96$ were treated as statistically distinguishable from zero at the 95% confidence level under the large-sample normal approximation. Contrasts were calculated at the factor-class level. If a single summary value is reported for a variable containing several classes, the aggregation rule must be stated explicitly because selecting a maximum, mean, or cumulative weight produces different interpretations.

3.7. Model Validation

Model validation distinguished overall map agreement from agreement in cells that changed. Kappa was used to compare the simulated and reference maps after adjustment for agreement expected by chance [97], [98].

$$Kappa\ (k) = \frac{(p_o - p_e)}{(1 - p_e)} \tag{13}$$

where (p_o) is the observed proportion of agreement and (p_e) is the agreement expected from the marginal class proportions. Kappa summarizes correspondence across the complete map; in a persistence-dominated setting, it can remain comparatively high even when newly converted cells are allocated incorrectly. It was therefore interpreted together with a change-specific measure rather than as a stand-alone acceptance criterion [79].

FoM evaluated the overlap between observed and simulated change:

$$FoM = \frac{B}{(A + B + C + D)} \times 100 \tag{14}$$

where (A) denotes observed change simulated as persistence (miss), (B) denotes observed change simulated correctly (hit), (C) denotes observed change simulated as an incorrect gaining category (wrong hit), and (D) denotes observed persistence simulated as change (false alarm). In a binary built-up/non-built-up model, (C) is absent unless the validation software retains a general multiclass formulation. FoM excludes correctly predicted persistence and is therefore more sensitive to the model's capacity to locate transition cells [80]. Kappa and FoM were reported jointly without using either statistic to infer causal validity.

4. RESULTS

4.1. Changes in Land Use and Land Cover Composition, 2005–2025

The land use and land cover (LULC) classification indicates a marked increase in the dominance of built-up land across the Makassar study area between 2005 and 2025 (Figure 5; Table 5). Across the seven LULC classes, the mapped study area remained constant at 17,590.87 ha in both observation years. Built-up land increased from 8,199.20 ha to 9,880.06 ha, representing a net gain of 1,680.86 ha, or 20.50% relative to its 2005 extent. Its share of the study area rose from 46.61% to 56.17%, an increase of 9.56 percentage points. Built-up land therefore shifted from being the largest individual LULC class to occupying more than half of the analyzed area.

Cropland experienced the largest absolute decline, decreasing by 861.81 ha from 4,967.83 ha to 4,106.02 ha. The next largest reductions occurred in water bodies (358.51 ha) and wetlands (249.36 ha); together, these two water-related classes lost a net 607.87 ha. Forest and grassland also declined by 144.71 ha and 125.49 ha, respectively. Among the contracting classes, grassland recorded the largest relative decrease (30.11%), followed by water bodies (29.58%).

Table 5. Changes in land use and land cover area, 2005–2025.

LULC class	2005 (ha)	2025 (ha)	Net change (ha)	Relative change (%)
Cropland	4,967.83	4,106.02	−861.81	−17.35
Forest	792.19	647.48	−144.71	−18.27
Shrubland	26.23	85.25	+59.02	+225.01
Grassland	416.80	291.31	−125.49	−30.11
Wetlands	1,976.48	1,727.12	−249.36	−12.62
Built-up land	8,199.20	9,880.06	+1,680.86	+20.50
Water bodies	1,212.14	853.63	−358.51	−29.58

LULC class	2005 (ha)	2025 (ha)	Net change (ha)	Relative change (%)
Total	17,590.87	17,590.87	0.00	0.00

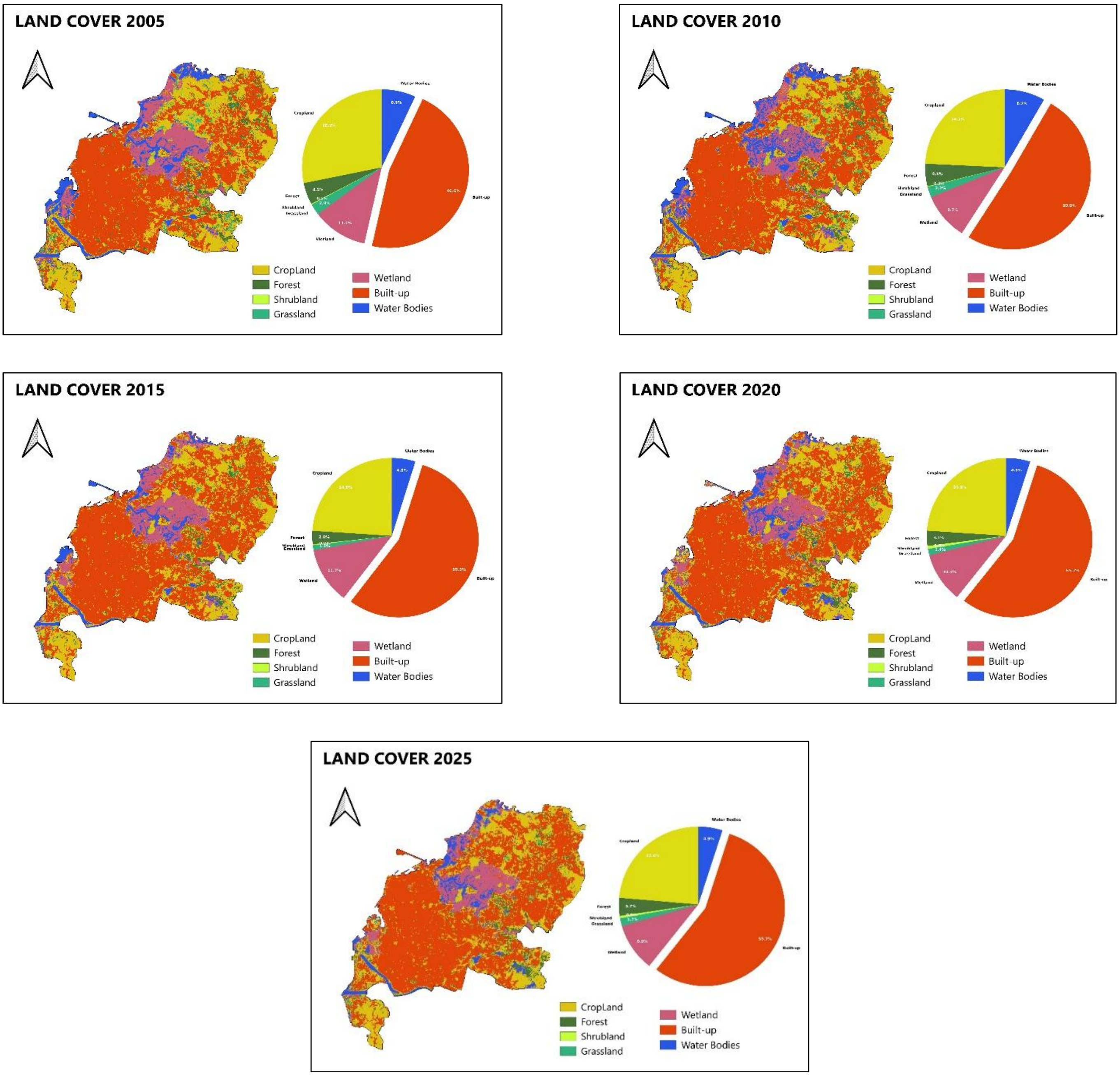

Figure 5. Spatial dynamics of land use and land cover in the Makassar study area in 2005, 2010, 2015, 2020, and 2025.

Shrubland was the only non-built-up class to increase, from 26.23 ha to 85.25 ha. Its 225.01% relative increase reflects the very small 2005 baseline; the absolute gain was only 59.02 ha. The percentage should therefore be interpreted together with the absolute change, whereas built-up expansion remained the dominant transformation of the study area.

The values in Table 5 represent net area change within each class and do not identify the source class of each newly built-up pixel. Without an interclass transition matrix, declines in cropland, water bodies, and wetlands cannot be attributed entirely to direct conversion into built-up land. Distinguishing net change from gross gain, gross loss, and interclass exchange is necessary to connect compositional change with specific land-transition processes [99].

4.2. Temporal Variation and Spatial Configuration

Built-up growth differed substantially between the two observation intervals of equal duration (Table 6; Figure 6). From 2005 to 2015, built-up area increased by 1,571.27

ha, from 8,199.20 ha to 9,770.47 ha. This corresponds to an average increase of 157.13 ha per year and a linear annual change rate of 1.916%. From 2015 to 2025, the net increase fell to 109.59 ha, equivalent to 10.96 ha per year and a linear annual rate of 0.112%.

Approximately 93.48% of the net built-up increase recorded during 2005–2025 occurred in the first interval. The net increase in the second interval was about 93.03% lower than that in the first. This contrast indicates a pronounced deceleration of horizontal expansion within the study boundary. Two decadal intervals, however, are insufficient to identify an annual structural breakpoint or to establish the causes of the deceleration statistically.

Figure 6 shows new built-up development along the existing urban edge and within gaps in established built-up areas, indicating spatial variation in growth location. Because edge expansion, infill, and isolated development were not quantified, the dominant growth mode and degree of spatial fragmentation cannot be determined.

Table 6. Change in built-up area across two observation intervals.

Period	Initial area (ha)	Final area (ha)	Net increase (ha)	Linear rate (% yr^{-1})
2005–2015	8,199.20	9,770.47	1,571.27	1.916
2015–2025	9,770.47	9,880.06	109.59	0.112

Note: Linear annual rate = 100 × (final area − initial area)/(initial area × interval length in years).

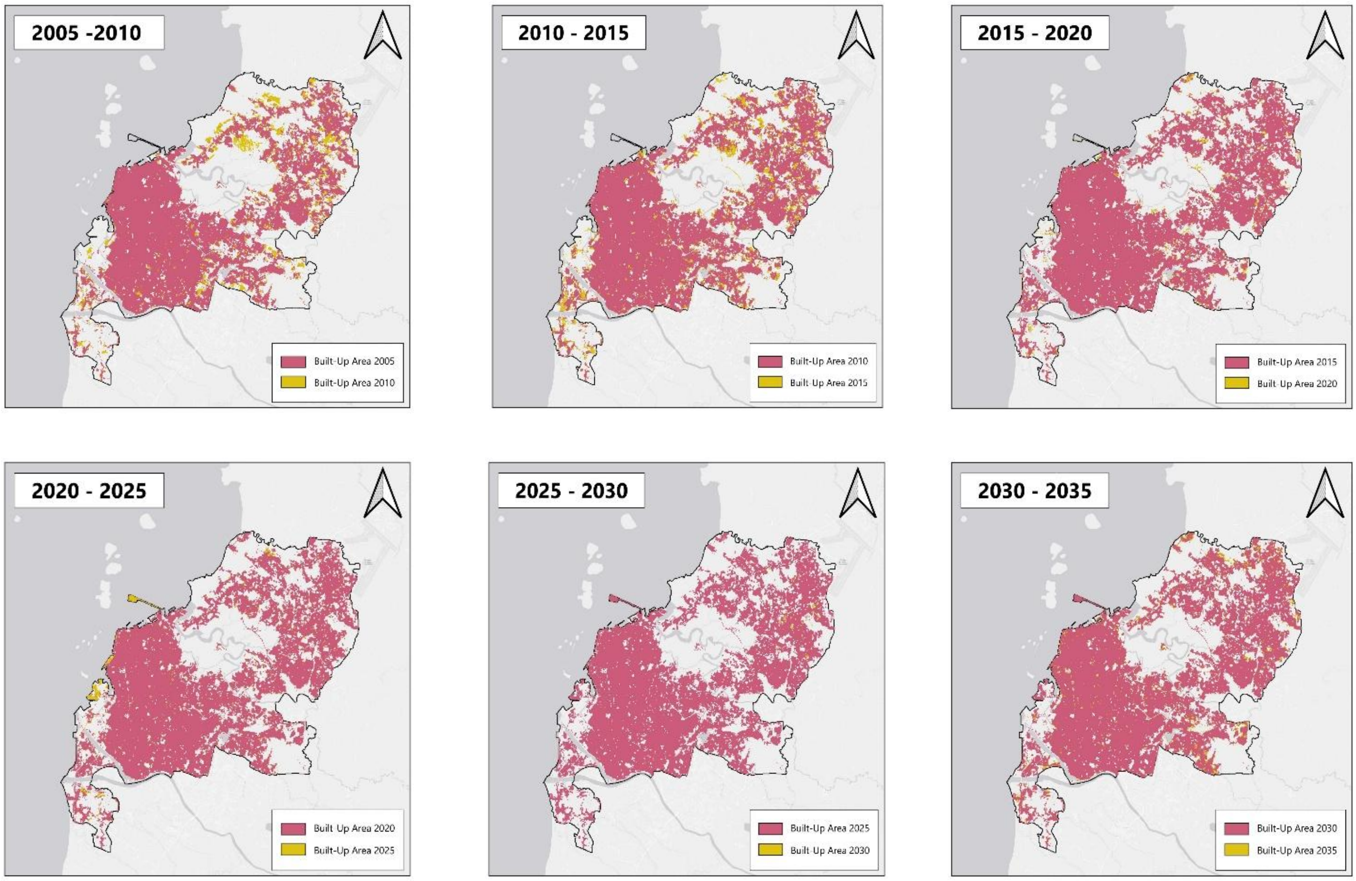

Figure 6. Spatial distribution of built-up expansion by five-year interval from 2005 to 2035. Intervals through 2025 are observed; intervals after 2025 are ANN–CA projections.

4.3. Spatial Associations of Driving Factors on WoE

The Weights of Evidence (WoE) analysis reports summary contrast values for ten variables representing demographic, economic, accessibility, environmental, and topographic conditions (Figures 7–8). Population growth has the largest reported positive summary value (C = +2.149), followed by land value (+1.663). Positive summaries are also reported for green/open-space proximity (+1.130), distance to economic centers (+0.764), distance to major roads (+0.750), distance to service centers (+0.599), and elevation (+0.337). The flood-exposure variable (labeled "Flood hazard" in the source output), distance to rivers, and population density have reported negative values of (−1.989), (−1.125) and (−0.904), respectively.

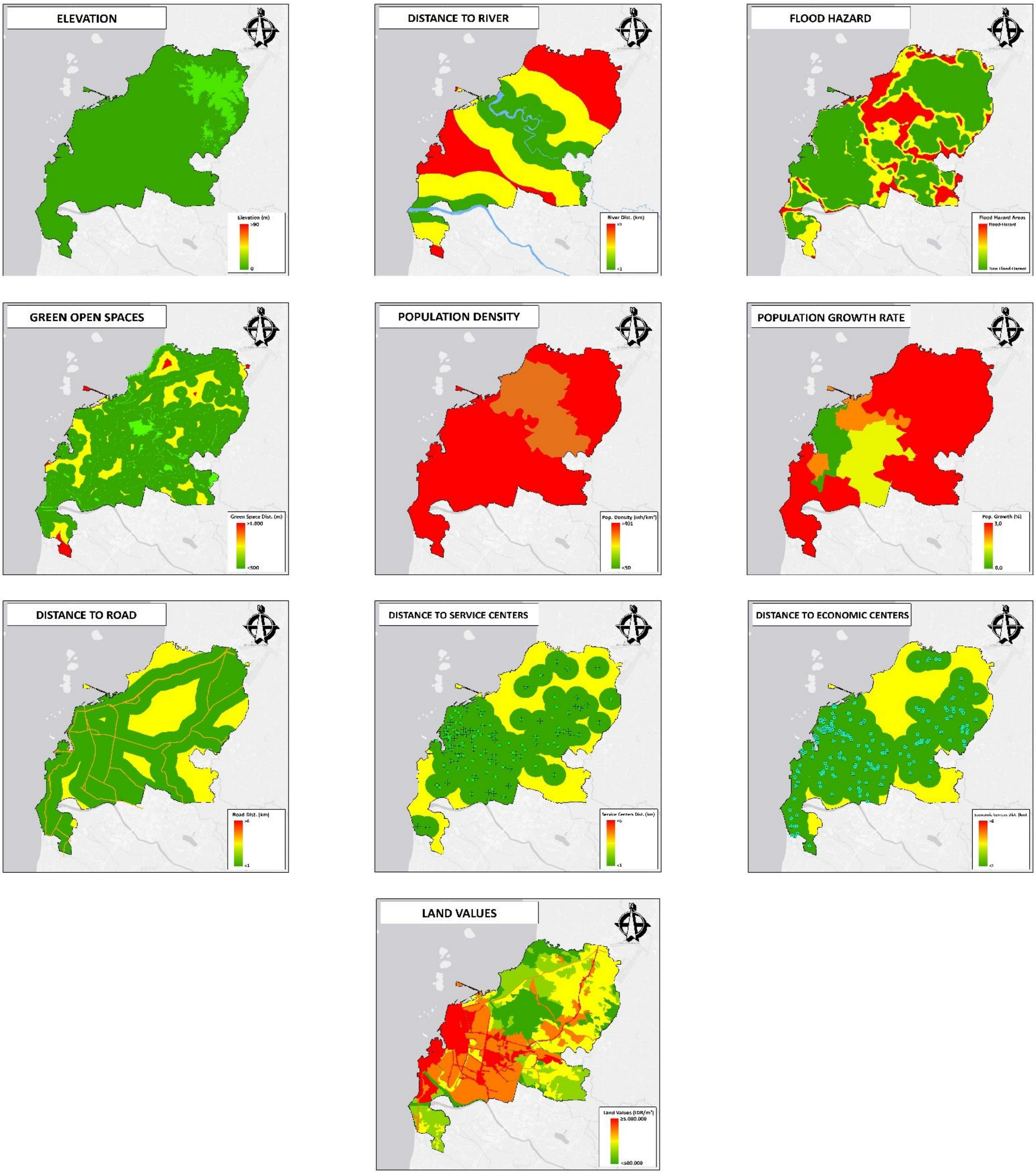

Figure 7. Spatial layers of the ten demographic, accessibility, economic, and physical-environmental drivers used in the urban-expansion model.

The opposite signs for population growth and population density are among the most prominent features of the WoE output (Figure 8). Population growth is positively associated with the summarized transition condition, whereas population density is negatively associated. The flood-exposure variable has the largest magnitude among the reported negative values, while elevation has the smallest positive value. This ordering is descriptive of the available C values and does not establish statistically significant differences in effect among the factors.

In WoE, contrast (C) is calculated for a specific factor class or condition [21]. Because the factor classes underlying the reported variable-level summary values are not provided, the sign of C cannot be interpreted as a monotonic relationship across the full range of a variable. A positive summary for a distance variable, for example, does not imply that expansion probability increases continuously with distance. (C) is also not a measure of internal predictor importance in the ANN.

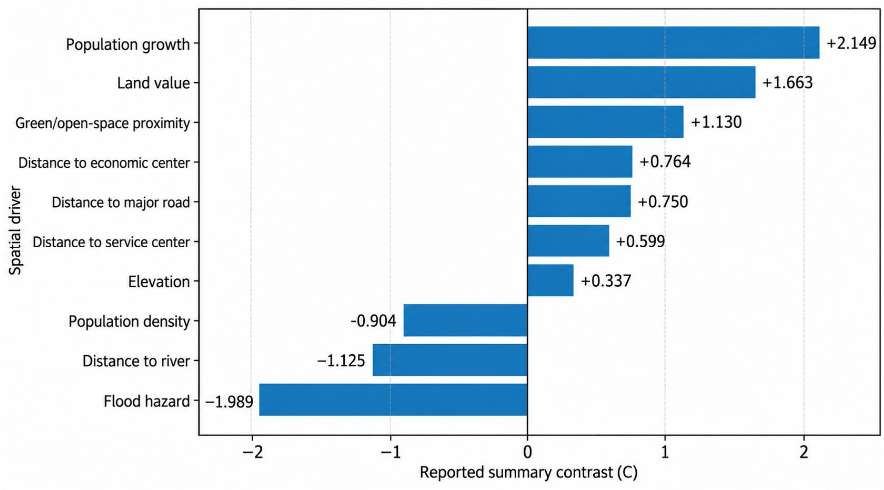

Figure 8. Reported variable-level Weights of Evidence (WoE) contrast summaries for built-up transition. Positive values indicate relative association with transition, and negative values indicate relative avoidance. The archived analytical record does not specify the factor-class aggregation rule; the source chart labels the flood-exposure variable as "Flood hazard."

4.4. Map Agreement and Locational Accuracy

Model evaluation reports a Kappa value of 0.768 and a Figure of Merit (FoM) of 21.01% (Table 7). These metrics address different aspects of model performance. Kappa summarizes categorical agreement between the model output and the reference map under its chance-agreement formulation.

Under the standard binary-change formulation, FoM is the ratio of correctly predicted change (hits) to the union of hits, observed changes that were missed (misses), and predicted changes that did not occur (false alarms). In multiclass evaluation, errors in the predicted destination class may also be incorporated, depending on the formulation used [80]. Accordingly, an FoM of 21.01% does not mean that 21.01% of the entire study area was predicted correctly, nor does it mean that the same proportion of all observed change was detected.

Taken together, the two metrics demonstrate why overall map agreement must be distinguished from the locational accuracy of change. A Kappa value of 0.768 is not sufficient evidence that the locations of new development were predicted accurately. Quantity and allocation disagreement should be separated to identify the sources of mismatch [24]. Because the FoM components, evaluation matrix, and validation reference year are unavailable, the contribution of each error component cannot be recalculated.

4.5. Projected Built-up Area through 2035

The ANN–CA simulation projects an increase in built-up land from the observed area of 9,880.06 ha in 2025 to 9,914.11 ha in 2030 and 10,394.23 ha in 2035 (Figure 9; Table 8). The projected decadal increase is therefore 514.17 ha, equivalent to 5.20% of the 2025 built-up area. Under a fixed study boundary, built-up land would occupy approximately 59.09% of the study area by 2035. The 2030 and 2035 maps retain the general spatial configuration of the existing urban area, although the extent of built-up land increases between the two projected states.

Table 7. Reported validation metrics for the ANN–CA model.

Indicator	Value	Measurement focus
Kappa	0.768	Categorical map agreement
Figure of Merit (FoM)	21.01%	Locational agreement of change

Table 8. Projected change in built-up area, 2025–2035.

Period	Initial area (ha)	Final area (ha)	Net increase (ha)	Linear rate (% yr^{-1})
2025–2030	9,880.06	9,914.11	34.05	0.069
2030–2035	9,914.11	10,394.23	480.12	0.969
2025–2035	9,880.06	10,394.23	514.17	0.520

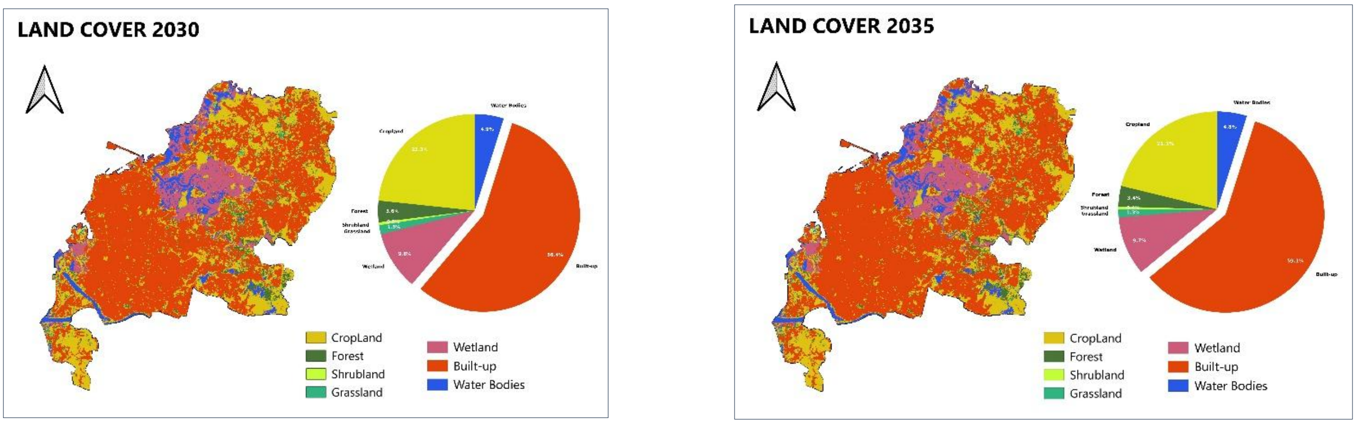

Figure 9. Projected land-use and land-cover distributions in 2030 and 2035 generated by the ANN–CA model.

Projected expansion is strongly uneven between the two five-year intervals. Built-up land increases by only 34.05 ha during 2025–2030, corresponding to 6.81 ha yr^{-1} and a linear rate of 0.069% yr^{-1}. The increase reaches 480.12 ha during 2030–2035, equivalent to 96.02 ha yr^{-1} and 0.969% yr^{-1}. Consequently, 93.38% of the projected 2025–2035 increase is allocated to the final five-year interval. The overall linear rate of 0.520% yr^{-1} exceeds the observed rate for 2015–2025 but remains below that recorded for 2005–2015.

The class-specific trajectories place the projected expansion within the longer-term LULC sequence (Figure 10). During the observed period from 2005 to 2025, built-up land increased progressively, whereas cropland exhibited the most persistent contraction. Wetland, water bodies, forest, and grassland also followed declining trajectories of varying magnitude, while shrubland remained comparatively stable. The projected 2030 and 2035 conditions maintain the general direction of these changes, although their temporal magnitudes differ substantially. The long-term trajectory is therefore characterized by class-specific land reallocation rather than proportional change across all LULC categories.

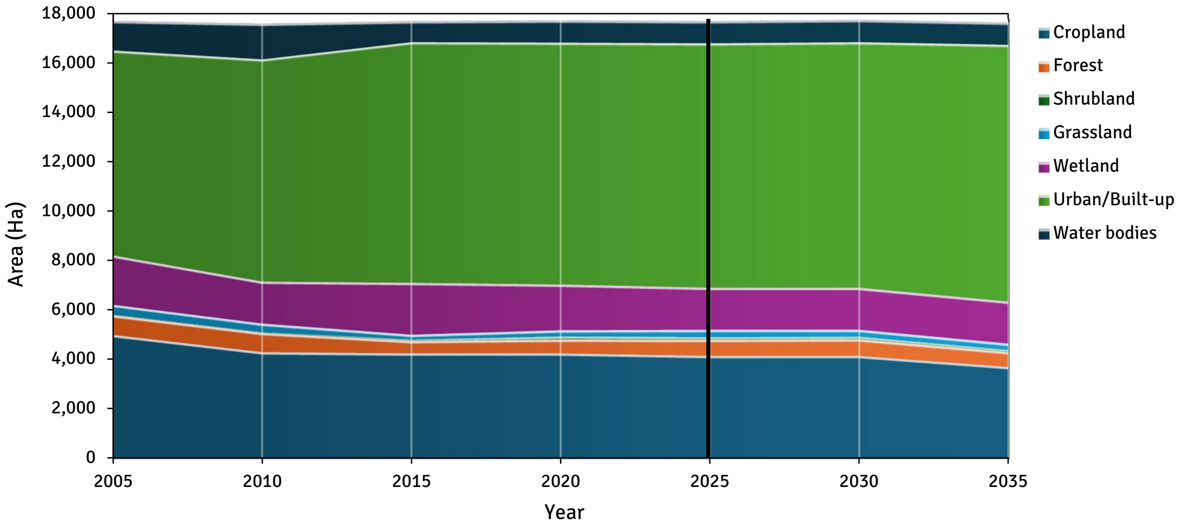

Figure 10. Temporal trajectories of land-use and land-cover class areas from 2005 to 2035. Observed values extend through 2025; values for 2030 and 2035 are ANN–CA projections.

Figure 11 summarizes observed net class changes between 2005 and 2025. Built-up land increased by 1,680.86 ha and shrubland by 59.02 ha, while cropland decreased by 861.81 ha, water bodies by 358.51 ha, wetlands by 249.36 ha, forest by 144.71 ha, and grassland by 125.49 ha. These values represent net class balances and do not identify the specific source-to-destination transitions responsible for the changes; such attribution requires a complete LULC transition matrix.

The interval-specific rates show substantial temporal heterogeneity in built-up expansion (Figure 12). The observed linear annual rate declined from 1.916% yr^{-1} during 2005–2015 to 0.112% yr^{-1} during 2015–2025. The model projects 0.069% yr^{-1} during 2025–2030 and 0.969% yr^{-1} during 2030–2035. The final projected interval therefore represents a reacceleration relative to the low-growth phase observed after 2015, while remaining below the 2005–2015 observed rate.

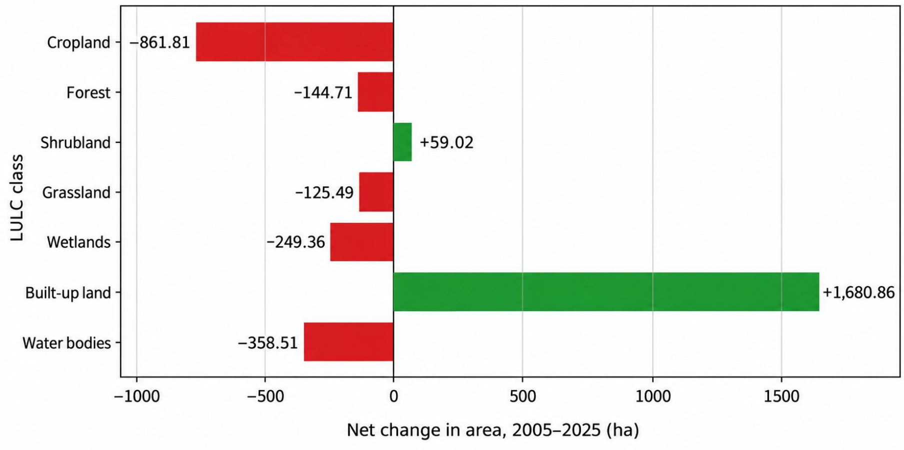

Figure 11. Observed net changes in land-use and land-cover class areas between 2005 and 2025.

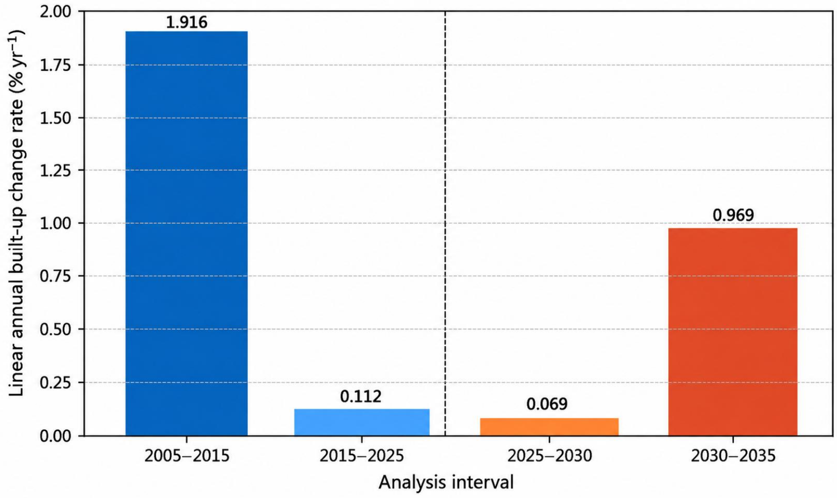

Figure 12. Linear annual rates of observed and projected built-up change by analysis interval.

The concentration of projected growth in 2030–2035 should be interpreted as a temporal allocation produced under the adopted model configuration. It does not establish that an equivalent acceleration in actual demographic growth, investment, infrastructure provision, or policy-driven development will occur during that interval. Without alternative land-demand scenarios, repeated simulations, and parameter-sensitivity analysis, the uncertainty surrounding the timing and magnitude of the projected expansion cannot be quantified.

5. DISCUSSION

5.1. Deceleration, Land Conversion and Demographic Differentiation of Urban Expansion

Urban expansion in Makassar exhibited marked temporal deceleration. Net built-up expansion declined from 1,571.27 ha during 2005–2015 to 109.59 ha during 2015–2025, while the linear annual expansion rate decreased from 1.916% to 0.112%. Therefore, 93.48% of the total built-up increase recorded between 2005 and 2025 occurred before 2015. A single long-term average would therefore obscure the temporal concentration of observed growth. Similar phase-dependent changes have been reported in cities undergoing shifts from rapid outward expansion toward more constrained or spatially selective development [37], [52], [100], [101]. Path-dependent urban configurations can also influence subsequent expansion opportunities and trajectories [102].

The observed deceleration is compatible with several mechanisms, including reduced availability of developable land, increasing infill, or redistribution of development toward peripheral areas. However, the present data cannot distinguish among these processes. The relative contribution of infill, edge expansion, and leapfrog development can change substantially over time and generate different implications for urban density and spatial continuity [102], [103]. Land markets, infrastructure provision, regulatory constraints, and institutional arrangements may also redirect development toward particular locations [2], [104], including cultivated peri-urban land where accessibility and development pressure intersect [57]. Slower expansion within the administrative boundary of Makassar may therefore represent either internal consolidation or displacement of development toward surrounding MAMMINASATA jurisdictions. Municipal containment should not automatically be interpreted as metropolitan containment because development pressure can cross administrative boundaries [100], [104]. Likewise, urban expansion is not equivalent to urban sprawl, which also involves density, fragmentation, continuity, and spatial configuration [102].

Built-up expansion was accompanied by substantial contraction of non-built-up classes. Cropland decreased by 861.81 ha, forest by 144.71 ha, grassland by 125.49 ha, wetlands by 249.36 ha, and water bodies by 358.51 ha. Cropland accounted for 49.53% of the combined net losses, indicating that agricultural land represents the largest component of the observed land-cover contraction. This pattern is consistent with broader evidence showing that urban expansion frequently occurs at the expense of productive peri-urban land [105] and can be associated with losses of habitat, biomass, and carbon storage [37]. These net balances, however, cannot establish direct transition pathways between individual land-cover classes. Net area change combines gains, losses, persistence, and spatial exchange, meaning that similar totals may result from substantially different transition processes [37], [99]. A pixel-level transition matrix is therefore required to identify the actual source and destination classes of urban conversion.

The combined decline of wetlands and water bodies reached 607.87 ha and is particularly relevant for urban planning. Interpretation requires caution because mapped changes in aquatic and wetland classes may be influenced by seasonal inundation, rainfall variability, acquisition dates, and spectral confusion [106]. If the decline represents persistent land-cover conversion, reduced water-storage capacity occurring simultaneously with increased impervious surfaces could increase runoff and flood exposure [107]–[109]. Spatial integration of observed transitions with hydrological and multi-hazard indicators would allow identification of locations where urban conversion overlaps with environmentally sensitive or hazard-prone areas [48]. The limited shrubland increase of 59.02 ha does not offset losses in other non-built-up classes. It may reflect secondary regrowth, land abandonment, management changes, or classification exchange rather than a systematic ecological recovery.

Demographic factors provide an additional explanation for the spatial differentiation of urban change. Population growth produced the strongest positive WoE contrast (+2.149), whereas population density showed a negative contrast (−0.904). These apparently opposing signals are conceptually consistent because population growth represents incremental demographic demand, whereas density represents the existing concentration of population. Previous research shows that urban land expansion responds differently to demographic change depending on metropolitan trajectory, city size, development stage, and spatial structure [5], [110]. Population increase and urban land expansion also show incomplete spatial correspondence globally [111], while urban growth can coexist with either increasing density through consolidation or declining density through outward extension [103], [112]. Comparative studies in Dar es Salaam, Tehran, and Puerto Rico similarly demonstrate that demographic growth does not generate a uniform spatial response [34], [51], [52]. Evidence from peri-urban Denpasar and Makassar likewise indicates that demographic change and land conversion are coupled but not equivalent processes [113], [114].

The negative association with population density is plausibly related to transition exposure. Highly populated cells may already contain extensive built-up surfaces, leaving limited land available for further conversion, whereas lower-density peripheral cells retain greater quantities of transition-eligible land. Initial land-cover conditions therefore shape the spatial opportunity structure available to land-change models [115]. Extension-oriented growth is also frequently associated with lower densities than compact or infill development [103], [110]. Population density should consequently be interpreted together with baseline land cover and the number of pixels eligible for transition rather than as an independent inhibitory mechanism.

These relationships remain associative rather than causal. WoE quantifies class-conditioned spatial associations and should not be interpreted as a regression coefficient, marginal effect, or monotonic causal response [21]. Statistical dependence between population growth and population density may also amplify combined evidence if predictor interactions are not adequately controlled [116]. The results identify a coordinated transition: rapid pre-2015 built-up expansion was followed by pronounced deceleration, losses were unevenly distributed among non-built-up classes, and population growth and density showed contrasting spatial associations with conversion. Distinguishing whether this pattern reflects urban consolidation, metropolitan spillover, or continued low-intensity dispersion requires explicit analysis of expansion morphology, baseline transition opportunities, and inter-jurisdictional development.

5.2. Spatial Drivers, Environmental Constraints and ANN–CA Model Performance

The WoE results indicate that urban expansion in Makassar reflects the combined influence of accessibility, land-market conditions, and environmental constraints. Land value produced the second-largest positive contrast (+1.663), while road accessibility and proximity to economic and service centers also showed positive associations with land conversion. This pattern is consistent with a market-access mechanism in which accessible locations with stronger economic connectivity become more attractive for development. However, relationships among land price, transport costs, and urban sprawl vary according to institutional and spatial contexts [64]. Accessibility has similarly been identified as an important determinant of urban land allocation elsewhere [57], but such comparative evidence does not independently establish the mechanism operating in Makassar.

Interpretation of land value also depends on temporal ordering. Development expectations may increase land prices before physical conversion occurs, whereas completed development can subsequently increase recorded land values. If the land-value surface corresponds to conditions measured during or after the modeled transition, the resulting WoE contrast may partly represent an outcome of urbanization rather than an antecedent driver. Land-value data should therefore be temporally aligned with the beginning of each calibration interval before directional influence is inferred. Distance-based variables require similar caution because WoE measures class-conditioned associations rather than continuous effects per kilometer and may exhibit non-monotonic responses among distance classes [21]. Class-specific WoE patterns, pixel frequencies, uncertainty intervals, and potential dependence among accessibility, centrality, and land value are therefore necessary for rigorous interpretation.

Environmental variables produced contrasting spatial signals. The flood-exposure variable showed the strongest negative WoE contrast (−1.989), followed by distance to rivers (−1.125). These values suggest that specific hydrological conditions were associated with reduced transition likelihood, but their meaning depends on the direction and thresholds used to define each factor class. They cannot be interpreted as evidence that all flood-prone areas or river corridors systematically resist urban conversion. Transition areas should therefore be examined within each hydrological class to determine whether development is concentrated in, excluded from, or redistributed among particular risk categories. This distinction is relevant because settlements frequently continue expanding into flood-prone areas despite recognized exposure [117]. A negative class-conditioned association in Makassar may consequently coexist with increasing aggregate flood exposure if development pressure remains sufficiently strong in selected high-risk locations.

Green/open-space proximity produced a reported positive WoE summary contrast (+1.130). In the operational definition used in Table 2, this predictor is represented as distance to protected/green open space; it should therefore be interpreted as a distance-class association rather than as direct evidence that the availability of green space promotes urban development. Protected green areas, formally planned open spaces, and vegetated but developable land may have different planning meanings. High ANN transition potential likewise does not establish ecological suitability or statutory developability. Integration with multi-hazard information can identify locations where projected growth conflicts with environmental constraints [48], so the projected map is more appropriate for spatial screening than for direct zoning or protection decisions.

These factor associations must be evaluated together with the predictive performance of the ANN–CA model. ANN–CA provides an appropriate framework for combining nonlinear transition learning with neighborhood-based spatial allocation, and previous Indonesian applications support its contextual relevance [19]. External precedent, however, cannot validate the Makassar model because model performance depends on local class composition, change prevalence, spatial extent, predictor structure, and validation design. Model credibility should therefore be assessed against locally observed land-use change rather than inferred from applications in other geographical contexts.

The reported Kappa value of 0.768 indicates whole-map correspondence, whereas the Figure of Merit (FoM) of 21.01% evaluates agreement specifically within changed locations. This distinction is critical because persistent cells can dominate whole-map agreement, particularly where the proportion of actual change is limited, while FoM is sensitive to the prevalence and location of observed transitions [25]. Component-based assessment can further distinguish correctly predicted changes from misses, false alarms, and allocation errors [80]. The combined metrics therefore indicate general similarity between observed and simulated maps but provide more limited confidence in the precise spatial allocation of newly built-up cells.

Accordingly, model performance is reported quantitatively without assigning qualitative performance categories to either Kappa or FoM. Kappa has recognized limitations as a stand-alone validation statistic and disagreement should be interpreted by separating change quantity from spatial allocation error [79]. A quantity–allocation decomposition and comparison with a no-change benchmark would provide a stronger test of whether ANN–CA improves prediction relative to retaining the 2025 land-use configuration.

Additional uncertainty arises from the temporal distribution of the projected built-up expansion. The model adds 514.17 ha of built-up land by 2035, but 480.12 ha, equivalent to 93.38% of the total projected increase, is allocated during 2030–2035, compared with only 34.05 ha during 2025–2030. This abrupt acceleration should not be interpreted as evidence of an expected economic or demographic surge because the available results do not establish such a mechanism. The discontinuity may instead arise from period-specific land-demand assumptions, spatial constraints, or nonlinear neighborhood interactions within the allocation process [79]. Explicit scenario analysis that varies land demand and planning restrictions would therefore provide a more defensible assessment of whether the projected post-2030 acceleration is robust to alternative modeling assumptions [65].

5.3. Planning Implications

Planning analysis should prioritize locations were transition potential overlaps cropland, wetlands, water bodies, or flood exposure. This follows directly from the observed 861.81-ha cropland decline and 607.87-ha water-related decline. Such overlays identify sites requiring review but do not constitute validated zoning. Scenarios should compare infill, edge, and peripheral growth by built-up increment, infrastructure demand, hazard exposure, and cropland retention. Open land may perform ecological or social functions [7], [105]; urban-growth-boundary studies demonstrate the value of varying land demand and spatial constraints before selecting a configuration [65].

Analysis should extend beyond Makassar to detect displacement into adjacent jurisdictions, consistent with the effects of metropolitan structure, policy, and commuting on sprawl [2]. The 2035 map remains conditional. Monitoring should track retained cropland, new hazard-zone development, infill share, and growth in infrastructure-served locations. These indicators would make the projection a falsifiable planning baseline and permit later assessment of whether growth is becoming more compact, less hazardous, and less land-consumptive.

5.4. Study Limitations and Contributions

LULC uncertainty is consequential because the 109.59-ha observed change during 2015–2025 and the 34.05-ha projection for 2025–2030 are small relative to the study area. Simulation Kappa cannot substitute for classification accuracy; probability sampling, class-specific accuracy, bias-adjusted area estimates, and confidence intervals remain necessary [118]. The archived classification records lack the underlying confusion matrices and weighting metadata, preventing independent reconstruction of reported OA, PA, and UA values from the displayed sample counts. Exact replication is also constrained by undocumented preprocessing details and ANN–CA implementation parameters, including factor classes, pixel counts, uncertainty in C, network architecture, data partitioning, validation year, neighborhood rules, and CA iterations. Random partitioning may inflate performance under spatial dependence, so validation should reflect spatial and temporal structure [119]. Transferability remains untested.

WoE identifies class-conditioned associations, while ANN–CA predicts and allocates change; neither establishes causal effects. The results identify four principal findings: post-2015 deceleration, unequal contraction of non-built-up classes, divergent demographic associations, and a gap between whole-map agreement and change-location accuracy. The integrated analysis therefore distinguishes conclusions supported directly by the observed data from those that remain conditional on model specification and incomplete validation metadata.

6. CONCLUSION

This study integrated multi-temporal land-use and land-cover (LULC) mapping, artificial neural network–cellular automata (ANN–CA) simulation, and Bayesian Weights of Evidence (WoE) analysis to reconstruct urban land transformation in Makassar during 2005–2025 and generate conditional projections for 2030 and 2035. Built-up land increased from 8,199.20 ha to 9,880.06 ha, representing a net gain of 1,680.86 ha or 20.50%. Its share of the study area rose from 46.61% to 56.17%. Expansion was temporally uneven, with 93.48% of the observed increase occurring during 2005–2015, followed by substantial deceleration. Cropland recorded the largest net decline at 861.81 ha, while wetlands and water bodies jointly decreased by 607.87 ha. These net balances do not establish direct conversion pathways without a complete interclass transition matrix.

WoE results identified population growth and land value as the strongest positive spatial associations, with contrast values of +2.149 and +1.663, whereas the flood-exposure variable showed the strongest negative association at −1.989. Because the underlying factor classes were not reported, these values represent class-conditioned associations rather than monotonic or causal effects. Validation yielded a Kappa coefficient of 0.768 and a Figure of Merit of 21.01%, indicating stronger whole-map agreement than change-specific locational accuracy.

Built-up land was projected to reach 10,394.23 ha by 2035, equivalent to 59.09% of the study area. However, 93.38% of projected growth occurred during 2030–2035, making the apparent acceleration dependent on model configuration. The projections should therefore be interpreted as conditional spatial-screening instruments, not deterministic forecasts or zoning prescriptions, given incomplete parameter reporting and the absence of comprehensive sensitivity analysis.

ACKNOWLEDGMENTS

The authors acknowledge the Department of Environmental Science, Post-Graduate Program, Hasanuddin University, for institutional and academic support, as well as colleagues who assisted throughout the research process.

CONFLICTS OF INTEREST

The authors declare that they have no competing interests or conflicts of interest related to this study.

DATA AVAILABILITY

The datasets generated and/or analyzed during this study are publicly available through the Open Science Framework (OSF) repository at https://doi.org/10.17605/OSF.IO/P3EYX. Additional information related to the datasets may be obtained from the corresponding author upon reasonable request.

ETHICAL STATEMENTS

Not applicable. This study did not involve any human participants or animals, and no personal or sensitive data were collected, used, or analyzed at any stage of the research. Field activities were limited to georeferenced land-cover observations used for remote-sensing classification and validation.

FUNDING

This research was conducted without financial support. The authors confirm that no funding was received for this study's research, analysis, or publication.

REFERENCES

[1] S. Angel, "Urban expansion: theory, evidence and practice," Build. Cities, vol. 4, no. 1, pp. 124–138, 2023, https://doi.org/10.5334/bc.348

[2] J. de Abreu e Silva and M. Correia, "The main drivers of urban sprawl in Portuguese medium cities between 2001 and 2011," Land use policy, vol. 132, p. 106803, 2023, https://doi.org/10.1016/j.landusepol.2023.106803

[3] X. Liu et al., "High-spatiotemporal-resolution mapping of global urban change from 1985 to 2015," Nat. Sustain., vol. 3, no. 7, pp. 564–570, 2020, https://doi.org/10.1038/s41893-020-0521-x

[4] R. Mahtta et al., "Urban land expansion: the role of population and economic growth for 300+ cities," npj Urban Sustain., vol. 2, no. 1, p. 5, 2022, https://doi.org/10.1038/s42949-022-00048-y

[5] K. C. Seto, M. Fragkias, B. Güneralp, and M. K. Reilly, "A meta-analysis of global urban land expansion," PLoS One, vol. 6, no. 8, p. e23777, 2011, https://doi.org/10.1371/journal.pone.0023777

[6] J. van Vliet, "Direct and indirect loss of natural area from urban expansion," Nat. Sustain., vol. 2, no. 8, pp. 755–763, 2019, https://doi.org/10.1038/s41893-019-0340-0

[7] K. C. Seto, B. Güneralp, and L. R. Hutyra, "Global forecasts of urban expansion to 2030 and direct impacts on biodiversity and carbon pools," Proc. Natl. Acad. Sci. U. S. A., vol. 109, no. 40, pp. 16083–16088, 2012, https://doi.org/10.1073/pnas.1211658109

[8] X. Liu, X. Li, Y. Chen, Z. Tan, S. Li, and B. Ai, "A new landscape index for quantifying urban expansion using multi-temporal remotely sensed data," Landsc. Ecol., vol. 25, no. 5, pp. 671–682, 2010, https://doi.org/10.1007/s10980-010-9454-5

[9] M. A. Wulder et al., "Current status of Landsat program, science, and applications," Remote Sens. Environ., vol. 225, pp. 127–147, 2019, https://doi.org/10.1016/j.rse.2019.02.015

[10] T. R. Loveland and J. R. Irons, "Landsat 8: The plans, the reality, and the legacy," Remote Sens. Environ., vol. 185, pp. 1–6, 2016. https://doi.org/10.1016/j.rse.2016.07.033

[11] X. Li and A. G. O. Yeh, "Neural-network-based cellular automata for simulating multiple land use changes using GIS," Int. J. Geogr. Inf. Sci., vol. 16, no. 4, pp. 323–343, 2002, https://doi.org/10.1080/13658810210137004

[12] L. Poelmans and A. Van Rompaey, "Detecting and modelling spatial patterns of urban sprawl in highly fragmented areas: A case study in the Flanders-Brussels region," Landsc. Urban Plan., vol. 93, no. 1, pp. 10–19, 2009, https://doi.org/10.1016/j.landurbplan.2009.05.018

[13] T. Basu, A. Das, and P. Pereira, "Exploring the drivers of urban expansion in a medium-class urban agglomeration in India using the remote sensing techniques and geographically weighted models," Geogr. Sustain., vol. 4, no. 2, pp. 150–160, 2023, https://doi.org/10.1016/j.geosus.2023.03.002

[14] D. R. Capozza and R. W. Helsley, "The fundamentals of land prices and urban growth," J. Urban Econ., vol. 26, no. 3, pp. 295–306, 1989, https://doi.org/10.1016/0094-1190(89)90003-X

[15] A. Sarkar and P. Chouhan, "Modeling spatial determinants of urban expansion of Siliguri a metropolitan city of India using logistic regression," Model. Earth Syst. Environ., vol. 6, no. 4, pp. 2317–2331, 2020, https://doi.org/10.1007/s40808-020-00815-9

[16] B. Güneralp, I. Güneralp, and Y. Liu, "Changing global patterns of urban exposure to flood and drought hazards," Glob. Environ. Chang., vol. 31, pp. 217–225, 2015, https://doi.org/10.1016/j.gloenvcha.2015.01.002

[17] K. M. Andreadis, O. E. J. Wing, E. Colven, C. J. Gleason, P. D. Bates, and C. M. Brown, "Urbanizing the floodplain: global changes of imperviousness in flood-prone areas," Environ. Res. Lett., vol. 17, no. 10, pp. 1–9, 2022, https://doi.org/10.1088/1748-9326/ac9197

[18] A. A. Kadhim, M. R. Aya, and Z. N. Jasim, "Flood Prone Areas Mapping Using Remote Sensing and GIS Techniques in Kalal Badrah Basin, Wasit, East of Iraq," J. Appl. Eng. Technol. Sci., vol. 7, no. 2, pp. 1550–1560, 2026, https://doi.org/10.37385/jaets.v7i2.9476

[19] M. H. Saputra and H. S. Lee, "Prediction of land use and land cover changes for North Sumatra, Indonesia, using an artificial-neural-network-based cellular automaton," Sustain., vol. 11, no. 11, p. 3024, 2019, https://doi.org/10.3390/su11113024

[20] T. Xu, D. Zhou, and Y. Li, "Integrating ANNs and Cellular Automata–Markov Chain to Simulate Urban Expansion with Annual Land Use Data," Land, vol. 11, no. 7, p. 1074, 2022, https://doi.org/10.3390/land11071074

[21] G. F. Bonham-Carter, Geographic Information Systems for Geoscientists. Oxford: Pergamon, 1994. https://doi.org/10.1016/c2013-0-03864-9

[22] H. Shafizadeh-Moghadam, A. Tayyebi, and M. Helbich, "Transition index maps for urban growth simulation: application of artificial neural networks, weight of evidence and fuzzy multi-criteria evaluation," Environ. Monit. Assess., vol. 189, no. 6, p. 300, 2017, https://doi.org/10.1007/s10661-017-5986-3

[23] H. Shafizadeh-Moghadam, M. Minaei, R. G. Pontius, A. Asghari, and H. Dadashpoor, "Integrating a Forward Feature Selection algorithm, Random Forest, and Cellular Automata to extrapolate urban growth in the Tehran-Karaj Region of Iran," Comput. Environ. Urban Syst., vol. 87, p. 101595, 2021, https://doi.org/10.1016/j.compenvurbsys.2021.101595

[24] R. G. Pontius and M. Millones, "Death to Kappa: Birth of quantity disagreement and allocation disagreement for accuracy assessment," Int. J. Remote Sens., vol. 32, no. 15, pp. 4407–4429, 2011, https://doi.org/10.1080/01431161.2011.552923

[25] R. G. Pontius et al., "Comparing the input, output, and

validation maps for several models of land change," Ann. Reg. Sci., vol. 42, no. 1, pp. 11–37, 2008, https://doi.org/10.1007/s00168-007-0138-2
[26] M. R. Abidin, R. Nur, E. M. Mayzarah, and R. Umar, "Estimating and Monitoring the Land Surface Temperature (LST) Using Landsat OLI 8 TIRS," Int. J. Environ. Eng. Educ., vol. 3, no. 1, pp. 17–24, 2021, https://doi.org/10.55151/ijeedu.v3i1.43
[27] M. I. Ali, G. D. Dirawan, A. H. Hasim, and M. R. Abidin, "Detection of changes in surface water bodies urban area with NDWI and MNDWI methods," International Journal on Advanced Science, Engineering and Information Technology, vol. 9, no. 3. pp. 946–951, 2019. https://doi.org/10.18517/ijaseit.9.3.8692
[28] T. Arifin et al., "Forecasting land-use changes due to coastal city development on the peri-urban area in Makassar City, Indonesia," Egypt. J. Remote Sens. Sp. Sci., vol. 26, no. 1, pp. 197–206, 2023, https://doi.org/10.1016/j.ejrs.2023.02.002
[29] E. E. Ramsay et al., "Spatio-temporal development of the urban heat island in a socioeconomically diverse tropical city," Environ. Pollut., vol. 316, p. 120443, 2023, https://doi.org/10.1016/j.envpol.2022.120443
[30] S. Wulandari, F. Pratama, N. Andika, P. Wongso, W. Wijayasari, and F. I. W. Rohmat, "Identifying dominant river contributions to urban flooding: a scenario-based study of Makassar City," Front. Built Environ., vol. 11, p. 1612416, 2025, https://doi.org/10.3389/fbuil.2025.1612416
[31] M. I. J. Putra and S. Phinn, "Integrating artificial neural network-cellular automata and bayesian weight of evidence for spatiotemporal analysis of urban change in Brisbane City," Comput. Urban Sci., vol. 6, no. 1, p. 13, 2026, https://doi.org/10.1007/s43762-026-00248-7
[32] R. M. Rosati, "Urban Sprawl and Routing: A Comparative Study on 156 European Cities," Landsc. Urban Plan., vol. 253, p. 105205, 2025, https://doi.org/10.1016/j.landurbplan.2024.105205
[33] L. N. Tellier, "Characterizing urban form by means of the Urban Metric System," Land use policy, vol. 111, p. 104672, 2021, https://doi.org/10.1016/j.landusepol.2020.104672
[34] S. Martinuzzi, W. A. Gould, and O. M. Ramos González, "Land development, land use, and urban sprawl in Puerto Rico integrating remote sensing and population census data," Landsc. Urban Plan., vol. 79, no. 3–4, pp. 288–297, 2007, https://doi.org/10.1016/j.landurbplan.2006.02.014
[35] A. El Garouani, D. J. Mulla, S. El Garouani, and J. Knight, "Analysis of urban growth and sprawl from remote sensing data: Case of Fez, Morocco," Int. J. Sustain. Built Environ., vol. 6, no. 1, pp. 160–169, 2017, https://doi.org/10.1016/j.ijsbe.2017.02.003
[36] S. Gaur, A. Mittal, A. Bandyopadhyay, I. Holman, and R. Singh, "Spatio-temporal analysis of land use and land cover change: a systematic model inter-comparison driven by integrated modelling techniques," Int. J. Remote Sens., vol. 41, no. 23, pp. 9229–9255, 2020, https://doi.org/10.1080/01431161.2020.1815890
[37] C. Wang et al., "Spatial-temporal patterns of urban expansion by land use/ land cover transfer in China," Ecol. Indic., vol. 155, p. 111009, 2023, https://doi.org/10.1016/j.ecolind.2023.111009
[38] R. Antonio Chaparro Torres, J. Wang, J. Zhang, L. Liu, and Y. Lan, "Temporal analysis of land degradation and urban expansion in central Yunnan Province using remote sensing for supporting sustainable development goals 11/15," Ecol. Indic., vol. 163, p. 112058, 2024, https://doi.org/10.1016/j.ecolind.2024.112058
[39] S. M. Sithole, W. Musakwa, J. Magidi, and A. Y. Kibangou, "Characterising landcover changes and urban sprawl using geospatial techniques and landscape metrics in Bulawayo, Zimbabwe (1984–2022)," Heliyon, vol. 10, no. 6, 2024, https://doi.org/10.1016/j.heliyon.2024.e27275
[40] M. R. Abidin and A. Arfan, "Detection of Development and Density Urban Build-Up Area with Satellite Image Overlay," Int. J. Environ. Eng. Educ., vol. 1, no. 2, pp. 40–45, 2019, https://doi.org/10.55151/ijeedu.v1i2.12
[41] S. Fazal, "The need for preserving farmland. A case study from a predominantly agrarian economy (India)," Landsc. Urban Plan., vol. 55, no. 1, pp. 1–13, 2001, https://doi.org/10.1016/S0169-2046(00)00134-1
[42] W. Song and X. Deng, "Land-use/land-cover change and ecosystem service provision in China," Sci. Total Environ., vol. 576, pp. 705–719, 2017, https://doi.org/10.1016/j.scitotenv.2016.07.078
[43] I. A. Festus, I. F. Omoboye, and O. B. Andrew, "Urban Sprawl: Environmental Consequence of Rapid Urban Expansion," Malaysian J. Soc. Sci. Humanit., vol. 5, no. 6, pp. 110–118, 2020, https://doi.org/10.47405/mjssh.v5i6.411
[44] B. F. Frimpong, A. Koranteng, and F. S. Opoku, "Analysis of urban expansion and its impact on temperature utilising remote sensing and GIS techniques in the Accra Metropolis in Ghana (1986–2022)," SN Appl. Sci., vol. 5, no. 8, p. 225, 2023, https://doi.org/10.1007/s42452-023-05439-z
[45] G. L. Vasárus, J. Z. Farkas, E. Hoyk, and A. D. Kovács, "The impact of urban sprawl on the urban-rural fringe of post-socialist cities in Central and Eastern Europe – Case study from Hungary," J. Urban Manag., vol. 13, no. 4, pp. 800–812, 2024, https://doi.org/10.1016/j.jum.2024.06.006
[46] M. Arvin, M. Jalaei, J. Taheri, B. Badakhshan, M. Ghane, and A. Sharifi, "Examining the relationship between urban form and social inequality: A neighborhood-level analysis," Appl. Geogr., vol. 176, p. 103532, 2025, https://doi.org/10.1016/j.apgeog.2025.103532
[47] S. Mansour, E. Ghoneim, A. El-Kersh, S. Said, and S. Abdelnaby, "Spatiotemporal Monitoring of Urban Sprawl in a Coastal City Using GIS-Based Markov Chain and Artificial Neural Network (ANN)," Remote Sens., vol. 15, no. 3, p. 601, 2023, https://doi.org/10.3390/rs15030601
[48] A. D. Sakti et al., "Machine learning based urban sprawl assessment using integrated multi-hazard and environmental-economic impact," Sci. Rep., vol. 14, no. 1, p. 13385, 2024, https://doi.org/10.1038/s41598-024-62001-6
[49] K. Ghasemi, A. M. Jarallah Al-Zubaidi, M. M. Qelichi, and K. Dolatkhahi, "Understanding urban sprawl in Baqubah, Iraq: A study of influential factors," J. Urban Manag., vol. 14, no. 3, pp. 787–812, 2025, https://doi.org/10.1016/j.jum.2025.01.013
[50] K. M. Almatar and M. F. Alhajri, "Drivers of urban sprawl in Dammam metropolitan area (DMA), Kingdom of Saudi Arabia: A qualitative exploration," J. Urban Manag., vol. 13, no. 3, pp. 469–481, 2024, https://doi.org/10.1016/j.jum.2024.06.003

[51] L. Congedo and S. Macchi, "The demographic dimension of climate change vulnerability: Exploring the relation between population growth and urban sprawl in Dar es Salaam," Curr. Opin. Environ. Sustain., vol. 13, pp. 1–10, 2015, https://doi.org/10.1016/j.cosust.2014.12.002

[52] H. Talkhabi, K. J. Ghalehteimouri, M. S. Mehranjani, A. Zanganeh, and T. Karami, "Spatial and temporal population change in the Tehran Metropolitan Region and its consequences on urban decline and sprawl," Ecol. Inform., vol. 70, p. 101731, 2022, https://doi.org/10.1016/j.ecoinf.2022.101731

[53] N. M. Sari, D. Kushardono, Mukhoriyah, Kustiyo, and M. D. M. Manessa, "an Optimized Artificial Neural Network for the Classification of Urban Environment Comfort Using Landsat-8 Remote Sensing Data in Greater Jakarta Area, Indonesia," J. Appl. Eng. Technol. Sci., vol. 4, no. 2, pp. 743–755, 2023, https://doi.org/10.37385/jaets.v4i2.1760

[54] Z. Wang, Q. Han, and B. de Vries, "Land Use/Land Cover and Accessibility: Implications of the Correlations for Land Use and Transport Planning," Appl. Spat. Anal. Policy, vol. 12, no. 4, pp. 923–940, 2019, https://doi.org/10.1007/s12061-018-9278-2

[55] Y. Liu, X. Cao, J. Xu, and T. Li, "Influence of traffic accessibility on land use based on Landsat imagery and internet map: A case study of the Pearl River Delta urban agglomeration," PLoS One, vol. 14, no. 12, p. e0224136, 2019, https://doi.org/10.1371/journal.pone.0224136

[56] D. Kasraian, K. Maat, D. Stead, and B. van Wee, "Long-term impacts of transport infrastructure networks on land-use change: an international review of empirical studies," Transp. Rev., vol. 36, no. 6, pp. 772–792, 2016, https://doi.org/10.1080/01441647.2016.1168887

[57] B. Rimal, H. Keshtkar, R. Sharma, N. Stork, S. Rijal, and R. Kunwar, "Simulating urban expansion in a rapidly changing landscape in eastern Tarai, Nepal," Environ. Monit. Assess., vol. 191, no. 4, p. 255, 2019, https://doi.org/10.1007/s10661-019-7389-0

[58] A. P. Pratama, M. H. Yudhistira, and E. Koomen, "Highway expansion and urban sprawl in the Jakarta Metropolitan Area," Land use policy, vol. 112, p. 105856, 2022, https://doi.org/10.1016/j.landusepol.2021.105856

[59] X. Zhu, T. Qian, and Y. Wei, "Do high-speed railways accelerate urban land expansion in China? A study based on the multi-stage difference-in-differences model," Socioecon. Plann. Sci., vol. 71, p. 100846, 2020, https://doi.org/10.1016/j.seps.2020.100846

[60] M. Aïkous, J. Dubé, C. Brunelle, and M. P. Champagne, "Is highway expansion and impacts on land use changes: An event study approach," Transp. Res. Part D Transp. Environ., vol. 119, p. 103730, 2023, https://doi.org/10.1016/j.trd.2023.103730

[61] M. Iacono and D. Levinson, "Mutual causality in road network growth and economic development," Transp. Policy, vol. 45, pp. 209–217, 2016, https://doi.org/10.1016/j.tranpol.2015.06.005

[62] J. Zhu, X. Niu, and Y. Wang, "Polycentric Urban Spatial Structure Identification Based on Morphological and Functional Dimensions: Evidence from Three Chinese Cities," Sustain. , vol. 16, no. 6, p. 2584, 2024, https://doi.org/10.3390/su16062584

[63] F. Hao, M. Lu, T. Yu, and S. Wang, "Identification and characterization of urban polycentric structure based on points of interest in Shenyang, China," Growth Change, vol. 55, no. 1, p. e12697, 2024, https://doi.org/10.1111/grow.12697

[64] H. Yu, S. Zhu, J. V. Li, and L. Wang, "Dynamics of urban sprawl: Deciphering the role of land prices and transportation costs in government-led urbanization," J. Urban Manag., vol. 13, no. 4, pp. 736–754, 2024, https://doi.org/10.1016/j.jum.2024.08.002

[65] X. Liang, X. Liu, X. Li, Y. Chen, H. Tian, and Y. Yao, "Delineating multi-scenario urban growth boundaries with a CA-based FLUS model and morphological method," Landsc. Urban Plan., vol. 177, pp. 47–63, 2018, https://doi.org/10.1016/j.landurbplan.2018.04.016

[66] Y. Li, J. Li, and J. Chu, "Research on land-use evolution and ecosystem services value response in mountainous counties based on the SD-PLUS model," Ecol. Evol., vol. 12, no. 10, p. e9431, 2022, https://doi.org/10.1002/ece3.9431

[67] C. M. Viana and J. Rocha, "Evaluating dominant land use/land cover changes and predicting future scenario in a rural region using a memoryless stochastic method," Sustain., vol. 12, no. 10, p. 4332, 2020, https://doi.org/10.3390/su12104332

[68] K. Jafarpour Ghalehteimouri, A. Shamsoddini, M. N. Mousavi, F. Binti Che Ros, and A. Khedmatzadeh, "Predicting spatial and decadal of land use and land cover change using integrated cellular automata Markov chain model based scenarios (2019–2049) Zarriné-Rūd River Basin in Iran," Environ. Challenges, vol. 6, p. 100399, 2022, https://doi.org/10.1016/j.envc.2021.100399

[69] N. R. Khwarahm, S. Qader, K. Ararat, and A. M. Fadhil Al-Quraishi, "Predicting and mapping land cover/land use changes in Erbil /Iraq using CA-Markov synergy model," Earth Sci. Informatics, vol. 14, no. 1, pp. 393–406, 2021, https://doi.org/10.1007/s12145-020-00541-x

[70] A. E. Al-Dousari, A. Mishra, and S. Singh, "Land use land cover change detection and urban sprawl prediction for Kuwait metropolitan region, using multi-layer perceptron neural networks (MLPNN)," Egypt. J. Remote Sens. Sp. Sci., vol. 26, no. 2, pp. 381–392, 2023, https://doi.org/10.1016/j.ejrs.2023.05.003

[71] W. Yue, C. Qin, M. Su, Y. Teng, and C. Xu, "Simulation and prediction of land use change in Dongguan of China based on ANN cellular automata - Markov chain model," Environ. Sustain. Indic., vol. 22, p. 100355, 2024, https://doi.org/10.1016/j.indic.2024.100355

[72] H. He and E. A. Garcia, "Learning from Imbalanced Data," IEEE Trans. Knowl. Data Eng., vol. 21, no. 9, pp. 1263–1284, 2009, https://doi.org/10.1109/TKDE.2008.239

[73] Y. Zhou, C. Huang, T. Wu, and M. Zhang, "A novel spatio-temporal cellular automata model coupling partitioning with CNN-LSTM to urban land change simulation," Ecol. Modell., vol. 482, p. 110394, 2023, https://doi.org/10.1016/j.ecolmodel.2023.110394

[74] G. Shmueli, "To explain or to predict?," Stat. Sci., vol. 25, no. 3, pp. 289–310, 2010, https://doi.org/10.1214/10-STS330

[75] S. Abdullahi and B. Pradhan, "Land use change modeling and the effect of compact city paradigms: integration of GIS-based cellular automata and weights-of-evidence techniques," Environ. Earth Sci., vol. 77, no. 6, art. 251, 2018, https://doi.org/10.1007/s12665-018-7429-z

[76] Y. Feng, R. Wang, X. Tong, and H. Shafizadeh-Moghadam, "How much can temporally stationary factors explain

cellular automata-based simulations of past and future urban growth?," Comput. Environ. Urban Syst., vol. 76, pp. 150–162, 2019, https://doi.org/10.1016/j.compenvurbsys.2019.04.010

[77] D. Lü, G. Gao, Y. Lü, Y. Ren, and B. Fu, "An effective accuracy assessment indicator for credible land use change modelling: Insights from hypothetical and real landscape analyses," Ecol. Indic., vol. 117, p. 106552, 2020, https://doi.org/10.1016/j.ecolind.2020.106552

[78] J. van Vliet, A. K. Bregt, and A. Hagen-Zanker, "Revisiting Kappa to account for change in the accuracy assessment of land-use change models," Ecol. Modell., vol. 222, no. 8, pp. 1367–1375, 2011, https://doi.org/10.1016/j.ecolmodel.2011.01.017

[79] X. Liu et al., "A future land use simulation model (FLUS) for simulating multiple land use scenarios by coupling human and natural effects," Landsc. Urban Plan., vol. 168, pp. 94–116, 2017, https://doi.org/10.1016/j.landurbplan.2017.09.019

[80] O. G. Varga, R. G. Pontius, S. K. Singh, and S. Szabó, "Intensity Analysis and the Figure of Merit's components for assessment of a Cellular Automata – Markov simulation model," Ecol. Indic., vol. 101, pp. 933–942, 2019, https://doi.org/10.1016/j.ecolind.2019.01.057

[81] M. I. Ali, A. H. Hasim, and M. R. Abidin, "Monitoring the built-up area transformation using urban index and normalized difference built-up index analysis," Int. J. Eng. Trans. B Appl., vol. 32, no. 5, pp. 647–653, 2019, https://doi.org/10.5829/ije.2019.32.05b.04

[82] A. M. Y. Hakim, S. Baja, D. A. Rampisela, and S. Arif, "Modelling land use/land cover changes prediction using multi-layer perceptron neural network (MLPNN): a case study in Makassar City, Indonesia," Int. J. Environ. Stud., vol. 78, no. 2, pp. 301–318, 2021, https://doi.org/10.1080/00207233.2020.1804730

[83] J. K. Gilbertson, J. Kemp, and A. van Niekerk, "Effect of pan-sharpening multi-temporal Landsat 8 imagery for crop type differentiation using different classification techniques," Comput. Electron. Agric., vol. 134, pp. 151–159, 2017, https://doi.org/10.1016/j.compag.2016.12.006

[84] Geospatial Information Agency of Indonesia, "Indonesian geospatial data and digital topographic map," Ina-Geoportal, 2025. https://tanahair.indonesia.go.id/portal-web/ (accessed Nov. 10, 2025).

[85] National Disaster Management Agency of Indonesia., "InaRISK," National Disaster Management Agency of Indonesia. https://inarisk.bnpb.go.id (accessed Nov. 10, 2025).

[86] Ministry of Forestry Republic of Indonesia "SIGAP Kehutanan: Geospatial Information System of the Ministry of Forestry," Ministry of Forestry. https://sigap.kehutanan.go.id (accessed Nov. 10, 2025).

[87] Central Bureau of Statistics (BPS) Makassar Municipality, Makassar Municipality in Figures 2025. Makassar: Central Bureau of Statistics (BPS), 2025. Accessed: Sep. 08, 2025. [Online]. Available: https://makassarkota.bps.go.id/id/publication/2025/02/28/81dcab96ca7120218f7f5fb3/kota-makassar-dalam-angka-2025.html

[88] OpenStreetMap contributors, "OpenStreetMap," OpenStreetMap. https://www.openstreetmap.org/ (accessed Sep. 08, 2025).

[89] Ministry of Agrarian Affairs and Spatial Planning/National Land Agency, "BHUMI ATR/BPN," Ministry of Agrarian Affairs and Spatial Planning/National Land Agency. https://bhumi.atrbpn.go.id (accessed Nov. 10, 2025).

[90] S. Fazal, "Land re-organisation in relation to roads in an Indian city," Land use policy, vol. 18, no. 2, pp. 191–199, 2001, https://doi.org/10.1016/S0264-8377(01)00007-2

[91] Q. Li, S. Thapa, X. Hu, Z. Luo, and D. J. Gibson, "The Relationship between Urban Green Space and Urban Expansion Based on Gravity Methods," Sustain., vol. 14, no. 9, p. 5396, 2022, https://doi.org/10.3390/su14095396

[92] A. Di Gregorio and L. J. M. Jansen, Land Cover Classification System (LCCS): Classification Concepts and User Manual. Rome, Italy: Food and Agriculture Organization of the United Nations (FAO), 2000. [Online]. Available: https://www.fao.org/4/x0596e/x0596e00.htm

[93] N. Gorelick, M. Hancher, M. Dixon, S. Ilyushchenko, D. Thau, and R. Moore, "Google Earth Engine: Planetary-scale geospatial analysis for everyone," Remote Sens. Environ., vol. 202, pp. 18–27, 2017, https://doi.org/10.1016/j.rse.2017.06.031

[94] L. Breiman, "Random Forests," Mach. Learn., vol. 45, no. 1, pp. 5–32, 2001, https://doi.org/10.1023/A:1010933404324

[95] S. V. Stehman and G. M. Foody, "Key issues in rigorous accuracy assessment of land cover products," Remote Sens. Environ., vol. 231, p. 111199, 2019, https://doi.org/10.1016/j.rse.2019.05.018

[96] L. Theres, S. Radhakrishnan, and A. Rahman, "Simulating Urban Growth Using the Cellular Automata Markov Chain Model in the Context of Spatiotemporal Influences for Salem and Its Peripherals, India," Earth (Switzerland), vol. 4, no. 2, pp. 296–314, 2023, https://doi.org/10.3390/earth4020016

[97] Y. Zhang, X. Liu, G. Chen, and G. Hu, "Simulation of urban expansion based on cellular automata and maximum entropy model," Sci. China Earth Sci., vol. 63, no. 5, pp. 701–712, 2020, https://doi.org/10.1007/s11430-019-9530-8

[98] J. Cohen, "A Coefficient of Agreement for Nominal Scales," Educ. Psychol. Meas., vol. 20, no. 1, pp. 37–46, 1960, https://doi.org/10.1177/001316446002000104

[99] R. G. Pontius, E. Shusas, and M. McEachern, "Detecting important categorical land changes while accounting for persistence," Agric. Ecosyst. Environ., vol. 101, no. 2–3, pp. 251–268, 2004, https://doi.org/10.1016/j.agee.2003.09.008

[100] J. Novotný, S. Chakraborty, and I. Maity, "Urban expansion of the 43 worlds' largest megacities: A search for unified macro-patterns," Habitat Int., vol. 129, p. 102676, 2022, https://doi.org/10.1016/j.habitatint.2022.102676

[101] S. Sadat Nickayin, L. Bianchini, G. Egidi, S. Cividino, K. Rontos, and L. Salvati, "'Pulsing' cities and 'swarming' metropolises: A simplified, entropy-based approach to long-term urban development," Ecol. Indic., vol. 136, p. 108605, 2022, https://doi.org/10.1016/j.ecolind.2022.108605

[102] L. Jiao, T. Dong, G. Xu, Z. Zhou, J. Liu, and Y. Liu, "Geographic micro-process model: Understanding global urban expansion from a process-oriented view," Comput.

Environ. Urban Syst., vol. 87, p. 101603, 2021, https://doi.org/10.1016/j.compenvurbsys.2021.101603
[103] G. Xu, Z. Zhou, L. Jiao, and R. Zhao, "Compact Urban Form and Expansion Pattern Slow Down the Decline in Urban Densities: A Global Perspective," Land use policy, vol. 94, p. 104563, 2020, https://doi.org/10.1016/j.landusepol.2020.104563
[104] A. Colsaet, Y. Laurans, and H. Levrel, "What drives land take and urban land expansion? A systematic review," Land use policy, vol. 79, pp. 339–349, 2018, https://doi.org/10.1016/j.landusepol.2018.08.017
[105] C. B. D'Amour et al., "Future urban land expansion and implications for global croplands," Proc. Natl. Acad. Sci. U. S. A., vol. 114, no. 34, pp. 8939–8944, 2017, https://doi.org/10.1073/pnas.1606036114
[106] J. F. Pekel, A. Cottam, N. Gorelick, and A. S. Belward, "High-resolution mapping of global surface water and its long-term changes," Nature, vol. 540, no. 7633, pp. 418–422, 2016, https://doi.org/10.1038/nature20584
[107] W. Handayani, U. E. Chigbu, I. Rudiarto, and I. H. Surya Putri, "Urbanization and increasing flood risk in the Northern Coast of Central Java-Indonesia: An assessment towards better land use policy and flood management," Land, vol. 9, no. 10, p. 343, 2020, https://doi.org/10.3390/LAND9100343
[108] B. Feng, Y. Zhang, and R. Bourke, "Urbanization impacts on flood risks based on urban growth data and coupled flood models," Nat. Hazards, vol. 106, no. 1, pp. 613–627, 2021, https://doi.org/10.1007/s11069-020-04480-0
[109] C. R. Jacobson, "Identification and quantification of the hydrological impacts of imperviousness in urban catchments: A review," J. Environ. Manage., vol. 92, no. 6, pp. 1438–1448, 2011, https://doi.org/10.1016/j.jenvman.2011.01.018
[110] B. Güneralp, M. Reba, B. U. Hales, E. A. Wentz, and K. C. Seto, "Trends in urban land expansion, density, and land transitions from 1970 to 2010: A global synthesis," Environ. Res. Lett., vol. 15, no. 4, p. 44015, 2020, https://doi.org/10.1088/1748-9326/ab6669
[111] J. Gao and B. O'Neill, "Different Spatiotemporal Patterns in Global Human Population and Built-Up Land," Earth's Futur., vol. 9, no. 8, p. e2020EF001920, 2021, https://doi.org/10.1029/2020EF001920
[112] S. Angel, P. Lamson-Hall, A. Blei, S. Shingade, and S. Kumar, "Densify and expand: A global analysis of recent urban growth," Sustain., vol. 13, no. 7, p. 3835, 2021, https://doi.org/10.3390/su13073835
[113] P. I. Christiawan and T. P. Lai Nguyen, "Re-Framing the Interlinked between Demographic Transition and Land-Use Change in Developing Countries Peri-urbanization," Indones. J. Geogr., vol. 56, no. 3, pp. 344–356, 2024, https://doi.org/10.22146/ijg.89118
[114] B. Surya, A. Salim, H. Hernita, S. Suriani, F. Menne, and E. S. Rasyidi, "Land use change, urban agglomeration, and urban sprawl: A sustainable development perspective of makassar city, indonesia," Land, vol. 10, no. 6, p. 556, 2021, https://doi.org/10.3390/land10060556
[115] P. H. Verburg, P. P. Schot, M. J. Dijst, and A. Veldkamp, "Land use change modelling: Current practice and research priorities," GeoJournal, vol. 61, no. 4, pp. 309–324, 2004, https://doi.org/10.1007/s10708-004-4946-y
[116] F. P. Agterberg and Q. Cheng, "Conditional independence test for weights-of-evidence modeling," Nat. Resour. Res., vol. 11, no. 4, pp. 249–255, 2002, https://doi.org/10.1023/A:1021193827501
[117] J. Rentschler et al., "Global evidence of rapid urban growth in flood zones since 1985," Nature, vol. 622, no. 7981, pp. 87–92, 2023, https://doi.org/10.1038/s41586-023-06468-9
[118] P. Olofsson, G. M. Foody, M. Herold, S. V. Stehman, C. E. Woodcock, and M. A. Wulder, "Good practices for estimating area and assessing accuracy of land change," Remote Sens. Environ., vol. 148, pp. 42–57, 2014, https://doi.org/10.1016/j.rse.2014.02.015
[119] D. R. Roberts et al., "Cross-validation strategies for data with temporal, spatial, hierarchical, or phylogenetic structure," Ecography (Cop.)., vol. 40, no. 8, pp. 913–929, 2017, https://doi.org/10.1111/ecog.02881

SUPPLEMENTARY

Table S1. Class-level training and validation sample sizes and reported classification accuracy by observation year.

Year	LULC class	Training (n)	Validation (n)	PA (%)	UA (%)
2005	Cropland	12	4	100.00	48.70
2005	Forest	22	9	58.11	66.67
2005	Shrubland	20	8	65.14	53.43
2005	Grassland	11	4	68.45	65.12
2005	Wetland	14	6	62.50	41.67
2005	Water bodies	27	11	76.56	85.96
2005	Urban/built-up	172	75	78.57	91.67
	Total (2005)	**278**	**117**		
2010	Cropland	12	5	100.00	52.50
2010	Forest	22	9	56.12	60.00
2010	Shrubland	20	8	54.23	55.23
2010	Grassland	11	4	63.33	40.00
2010	Wetland	14	6	77.50	37.50
2010	Water bodies	27	11	82.81	88.33
2010	Urban/built-up	167	71	100.00	67.78
	Total (2010)	**273**	**114**		
2015	Cropland	12	5	100.00	62.50
2015	Forest	22	9	69.09	53.33
2015	Shrubland	20	8	72.50	100.00
2015	Grassland	11	4	56.67	53.33
2015	Wetland	14	6	52.50	53.33
2015	Water bodies	27	11	92.19	88.06
2015	Urban/built-up	177	81	57.14	100.00
	Total (2015)	**283**	**124**		
2020	Cropland	12	5	100.00	63.33
2020	Forest	22	9	54.55	85.71
2020	Shrubland	20	8	60.00	100.00
2020	Grassland	11	4	73.33	100.00
2020	Wetland	14	6	62.50	55.71
2020	Water bodies	27	11	89.06	93.44
2020	Urban/built-up	162	66	64.29	90.00
	Total (2020)	**268**	**109**		
2025	Cropland	5	1	100.00	22.22
2025	Forest	22	9	72.73	80.00
2025	Shrubland	20	8	75.00	100.00
2025	Grassland	11	4	83.33	100.00
2025	Wetland	14	6	75.00	66.67
2025	Water bodies	27	11	90.62	96.67
2025	Urban/built-up	169	72	100.00	100.00
	Total (2025)	**268**	**111**		

Note: PA = Producer's Accuracy; UA = User's Accuracy. Values are retained from the archived classification records. The class-level confusion matrices, denominators used for each accuracy statistic, and any sampling or area-weighting scheme were not retained; PA and UA therefore cannot be independently reconstructed from the displayed validation sample counts alone.